

Small x physics and RHIC data

T. Lappi

*Physics Department, P.O. Box 35, 40014, University of Jyväskylä, Finland and
Helsinki Institute of Physics, P.O. Box 64, 00014 University of Helsinki, Finland
tuomas.lappi@jyu.fi*

This is a review of applications of the Color Glass Condensate to the phenomenology of relativistic heavy ion collisions. The initial stages of the collision can be understood in terms of the nonperturbatively strong nonlinear glasma color fields. We discuss how the CGC framework can and has been used to compute properties of the initial conditions of AA collisions. In particular this has led to recent progress in understanding multiparticle correlations, which can provide a directly observable signal of the properties of the initial stage of the collision process.

2 *T. Lappi*

Contents

1	Introduction	3
2	Glasma initial state	5
2.1	Description of a nucleus in the CGC	5
2.2	Glasma fields	7
2.3	Factorization	12
3	Nuclear wavefunction	13
3.1	Deep inelastic scattering	13
3.2	Proton-nucleus collisions	15
3.3	Dipole cross section parametrizations	17
4	Bulk gluon production in nucleus-nucleus collisions	19
4.1	Calculating the initial gluon multiplicity	20
4.2	Energy and rapidity dependence	22
5	Transverse geometry	23
5.1	Centrality dependence of multiplicity	24
5.2	Eccentricity of the initial state	25
6	Correlations in the glasma	27
6.1	Multigluon correlations in the boost invariant case	29
6.2	The ridge and the negative binomial	32
6.3	Chiral magnetic effect	35
6.4	Rapidity dependence of two gluon correlation	36
7	Conclusions	39

1. Introduction

The Relativistic Heavy Ion collider (RHIC) at Brookhaven National Laboratory has been taking data from nucleus-nucleus, deuteron-nucleus and proton-proton collisions starting from 2000. This successful program has provided a wealth of information on the properties of QCD matter at high energy density. For a review of the early experimental results we refer the reader to the experimental “white papers”¹ by the RHIC collaborations. Since the earliest RHIC observations it has become clear that the produced matter is deconfined and cannot be understood in terms of phenomenological models of low energy hadron physics. It is obvious that this will be even more true for heavy ion collisions at the LHC. On the other hand, there are many signs that the matter interacts far too strongly to be described by naive perturbative calculations. The first principles method of studying nonperturbative QCD is to directly discretize the path integral on a lattice and evaluate it numerically. This is indeed the method of choice for the description of a static system, such as studying the equation of state. The lattice, however, is ill suited for understanding time dependent phenomena, and other methods must be developed. One is then faced with a choice between two views, depending on whether “strongly interacting” in the context of gauge theory implies a large value of the coupling constant α_s or not. One option is that one should consider α_s to be large. Performing practical computations in this strong coupling limit has now become possible at least in some nonabelian gauge theories, if not yet in QCD, due to a duality transformation that makes it possible to translate the problem into solving a classical wave equation in 5 dimensional gravity². There has been much activity in this direction recently, and gauge/gravity duality seems a promising tool to gain qualitative understanding of the properties of the medium in the plasma phase.

A strong coupling theory fails, however, in describing some basic features of high energy hadronic collisions that characterize the initial stage of a heavy ion collision. The predominance of forward scattering in the angular distribution (i.e. the approximate boost invariance of particle production, the small baryon stopping in hadronic collisions, the existence of jets) point towards an interaction that is well described by a weak coupling gauge theory (see e.g. the discussion in³). This leads to the point of view that we will assume in this paper; namely that for the initial conditions of heavy ion collisions the system can be described assuming that α_s is small. In spite of the coupling constant being small the system can be strongly interacting because it is dense; gluonic states have high occupation numbers and the interactions between them are highly nonlinear. One possible application of this idea is to assume the existence of a geometrical condition that restricts the number of particles in the central rapidity region when they begin to overlap in phase space. In a practical phenomenological application one can then first calculate the initial production of partons using a framework developed for a generic hadronic collision and then supplement this calculation with the geometric (“final state”) saturation criterion. Examples of this line of reasoning are provided e.g. by the

EKRT model⁴, which uses the usual collinear pQCD factorization, or the parton percolation model⁵, based on string-like phenomenology. The line of thought that we will pursue here, however, is that the nonlinear interactions that control the behavior of the bulk of particle production are present already in the initial nuclear wavefunction⁶ and lead to the emergence of an (“initial state”) *saturation scale*; a transverse momentum scale that then manifests itself in particle production in the collision.

In collisions of protons and nuclei the typical values of x that are probed in the wavefunction are $x \sim p_T/\sqrt{s}$, where p_T is a typical transverse momentum scale of the particles being produced. Let us consider, in the center-of-mass frame of the collision, the nucleus moving in the $+z$ direction. The parton with momentum fraction x will have longitudinal momentum $p^+ \sim x\sqrt{s}/A$ and will thus probe the other, leftmoving, nucleus at a length scale $\Delta x^- \sim A/(x\sqrt{s})$. The longitudinal size of the leftmover is Lorentz-contracted from $R_A \sim A^{1/3}R_p$ to $\sim A^{1/3}R_p(Am_N/\sqrt{s})$. We see that if $x \ll 1/(A^{1/3}R_p m_N)$, the partons in the rightmoving nucleus will not be able to resolve the individual nucleons of the leftmoving one. The whole nucleus must therefore be treated as one coherent target, not as a collection of independent nucleons.

The observation that the large x localized, valence-like, degrees of freedom are not resolved in the collision, but only the smaller x partons that they radiate, naturally leads to the idea of treating the two separately in an effective field theory approach. This effective field theory is known as the Color Glass Condensate (CGC)^{7,8} (see⁹ for reviews and¹⁰ for a summary of the case for the CGC based on RHIC data.). The CGC describes a high energy hadron in terms of a color field (the small x gluons) radiated by an effective color current (the large x degrees of freedom). At high energy (small x) the radiation is enhanced by large logarithms of the energy and the number of gluons is large. When the occupation numbers of gluonic states in the wavefunction becomes large enough, $\sim 1/\alpha_s$, the field can be described as a classical one, radiated by classical effective color charges. The classical color charges are stochastic random variables with a probability distribution $W_x[\rho]$. Both the properties of the initial stage of a heavy ion collision and observables in DIS at small x can be computed in terms of these same classical gluon fields. The color charge distribution depends on nonperturbative input and cannot completely be computed from first principles. Its dependence on the energy scale (rapidity) that separates the large and small x degrees of freedom can, however, be computed and expressed in terms of a renormalization group equation. The distribution of color charges is a universal object; it can be measured in one process (ideally DIS) and then used as an independent input to make prediction for another one (say, the initial field configurations in a heavy ion collision). In this sense the situation is analogous to collinear factorized perturbation theory; there is a universal, nonperturbative distribution (color charge distribution or parton distribution function), a separation scale (rapidity or virtuality) and a renormalization group equation derived from

first principles that describes the dependence of the nonperturbative input on this separation scale.

2. Glasma initial state

We now turn to the basic features of the glasma¹¹ fields in the initial stages of the collision. We shall show how their structure as initially longitudinal boost invariant fields follows directly from the CGC description of the nuclear wavefunction.

2.1. Description of a nucleus in the CGC

In the CGC picture the small x degrees of freedom that contribute to bulk gluon production are treated as a classical color field radiated by (classical) color sources. As classical fields they obey the Yang-Mills equation of motion

$$[D_\mu, F^{\mu\nu}] = J^\nu, \quad (1)$$

with the source currents

$$J^\mu = \delta^{\mu+} \rho_1(\mathbf{x}_T, x^-) + \delta^{\mu-} \rho_2(\mathbf{x}_T, x^+) \quad (2)$$

representing the large x part of the wavefunctions. The color charge densities are *static* in the sense that they do not depend on the relevant light cone time (x^\pm for $\rho_{1,2}$ respectively). The color charges of the two nuclei are naturally independent of each other. They are also localized on their respective light cones: $\rho_{1,2}(\mathbf{x}_T, x^\mp) \sim \rho_{1,2}(\mathbf{x}_T) \delta(x^\mp)$. A naive way to understand this dependence is to argue that at high energy the nuclei are Lorentz-contracted to infinitesimal sheets in an interval^a $\Delta x^- \sim 1/\sqrt{s}$. This argument does not, however, take into account the quantum nature of the color charged integrated into the effective description in terms of the ρ 's. The color charge densities represent degrees of freedom that have a higher x , i.e. a higher longitudinal momentum p^+ than the ones described as the classical field. Consequently they are better localized in x^- (the conjugate variable to p^+) than the classical field and are, in the high energy (multi-Regge) kinematics we are working in, seen by the glasma field as infinitesimal sheets. The actual scale of this delta function can be estimated as follows. The longitudinal (and transverse) momenta of the gluons in the classical field are^b $\sim Q_s$. The evolution speed in rapidity is proportional to α_s ; we can therefore assume that the sources are separated from the classical field by $\Delta y \sim 1/\alpha_s$ units in rapidity. Thus they correspond to longitudinal momenta $p^+ \sim e^{1/\alpha_s} Q_s$, i.e. are localized in an interval $\Delta x^- \sim e^{-1/\alpha_s}/Q_s$. This is the actual meaning of the delta function approximation used when writing $\rho_1(\mathbf{x}_T, x^-) \sim \rho_1(\mathbf{x}_T) \delta(x^-)$. As we shall see in the following, it is nevertheless important to initially maintain an explicit x^- -dependence in the color

^aWe're concentrating for the moment on the rightmoving nucleus.

^bWe are assuming that one is here interested in the field around $y = 0$, otherwise all the scales in the following argument must be boosted appropriately.

6 *T. Lappi*

charge density and only take the δ -function limit later at the appropriate stage. In the leading logarithmic kinematics the x^- -dependence will be identified with the dependence of the color charge density on the rapidity (or x) at which it is probed.

The computation of the glasma fields from the current (2) proceeds in the following way¹². One must first solve the problem for the field of one individual nucleus; the gauge fields of the individual nuclei will then give the initial condition for computing the field configuration in a two-nucleus collision. We shall first go through these small manipulations that will give us a picture of the initial glasma field configurations after the collision before discussing the relation to the renormalization group evolution of the sources.

The solution for the color current of one nucleus

$$J^\mu = \delta^{\mu+} \rho_1(\mathbf{x}_T, x^-) \quad (3)$$

is most easily found in the covariant gauge $\partial_\mu A_{\text{cov}}^\mu = 0$. One can find a solution with only one component of the gauge field is nonzero, namely $A_{\text{cov}}^+(\mathbf{x}_T, x^-)$. In this case Eq. (1) becomes a 2-dimensional Poisson equation

$$-\nabla_T^2 A_{\text{cov}}^+ = \rho(\mathbf{x}_T, x^-), \quad (4)$$

for which we can formally write the solution as

$$A_{\text{cov}}^+ = -\rho(\mathbf{x}_T, x^-)/\nabla_T^2. \quad (5)$$

Note that there is an infrared singularity in Eq. (5). The most natural prescription to invert the Laplacian ∇_T^2 is to impose the constraint $\int d^2\mathbf{x}_T \rho(\mathbf{x}_T) = 0$, i.e. to require that the source as a whole is color neutral. Imposing color neutrality at a shorter length scale will also remove this ambiguity.

The covariant gauge solution has the advantage of being localized on the light cone in the t, z -plane, but its interpretation in terms of partons is not very clear. To interpret the classical field in terms of quasi-real Weizsäcker-Williams gluons we must transform the field into the light cone (LC) gauge. This gauge transformation can be done using the path ordered exponential

$$U(\mathbf{x}_T, x^-) = \text{P exp} \left\{ ig \int_{-\infty}^{x^-} dy^- A_{\text{cov}}^+(\mathbf{x}_T, y^-) \right\}, \quad (6)$$

giving

$$A_{\text{LC}}^\pm = 0 \quad (7)$$

$$A_{\text{LC}}^i = \frac{i}{g} U(\mathbf{x}_T, x^-) \partial_i U^\dagger(\mathbf{x}_T, x^-). \quad (8)$$

The light cone gauge solution is not localized on the x^+ -axis, unlike the one in covariant gauge. Instead, it extends to the whole region $x^- > 0$ as a transverse pure gauge field. The field strength tensor $F^{\mu\nu}$, however is nonzero only on the light cone $x^- = 0$ because there is a nonzero energy density only following the color source.

In general the color charge densities are stochastic random variables drawn from some distribution $W_y[\rho]$. This probability distribution cannot be computed from first principles, but its dependence on y can; it is given by the JIMWLK renormalization group equation, which we shall return to shortly. For many phenomenological applications and the following discussion, it will be enough to consider the distribution defined by the McLerran-Venugopalan (MV) model¹³, which could be considered as a reasonable initial condition for JIMWLK. In the MV model the color charges are distributed with the Gaussian probability distribution

$$\langle \rho^a(\mathbf{x}_T, x) \rho^b(\mathbf{y}_T, y) \rangle = g^2 \mu_A^2 \delta^{ab} \delta^2(\mathbf{x}_T - \mathbf{y}_T) \delta(x^- - y^-). \quad (9)$$

One can motivate the simple Gaussian approximation by an argument that is essentially based on the central limit theorem. The classical color charge density in the CGC is conceptually a sum of the color charges of all the higher x partons that have been integrated out of the theory. If these color charges are uncorrelated (incoherent) and there are sufficiently many of them, the resulting distribution will be Gaussian¹⁴ and local in transverse space. This assumption of independent color charges adding up to the effective charge $\rho(\mathbf{x}_T)$ also leads to the assumption that the parameter μ^2 should be proportional to the thickness of the target (i.e. $\mu^2 \sim A^{1/3}$); a dependence that is modified by quantum evolution that introduces correlations between the charges^{15,16}. The MV model has two important properties that we must mention here. Firstly, as originally shown in Ref.⁷, it leads to *saturation* of the unintegrated gluon distribution (and of the dipole cross section), at transverse momentum scales $k_T \lesssim Q_s \sim g^2 \mu$ (we shall comment on the precise relation between $g^2 \mu$ and Q_s later, see also^{17,18}). Secondly, in the dilute large transverse momentum limit it leads to an unintegrated gluon distribution that behaves as $\sim 1/k_T^2$. In terms of the integrated distribution this means that $xG(x, Q^2) \sim \ln Q^2$, the kind of generic behavior one expects from DGLAP evolution. These two features; saturation and a perturbative-like gluon spectrum at large \mathbf{k}_T , make it reasonable to expect that the MV model should be a realistic one for phenomenology at RHIC energies, where the effects of JIMWLK evolution have not yet drastically modified the distribution of the color charges.

2.2. Glasma fields

Let us then turn to the case of two colliding nuclei. It is more convenient here to work in an axial gauge. The reason for this is that we would like to understand the solution of the classical equations of motion inside the future light cone $\tau > 0$ as an *initial value problem* involving only the initial conditions of the fields A_μ at $\tau = 0$ and subsequent propagation into the vacuum. If one studies the solution of the two nucleus problem in the covariant gauge the large A^+ -component of the *field* of the rightmoving source causes a precession (due to covariant current conservation $[D_\mu, J^\mu] = 0$) of the *current* of the leftmoving nucleus. Thus in the covariant gauge an essential part of the interaction involves the currents directly. In a light cone

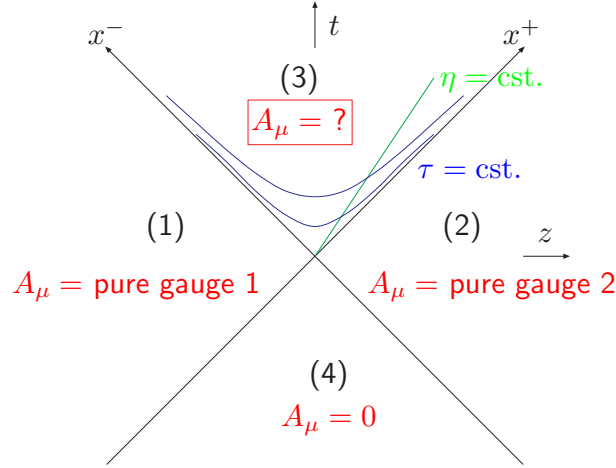


Fig. 1. Color fields in spacetime. In regions (1) and (2), where only one of the nuclei has passed by, the field is the pure gauge field of this one nucleus. In region (3) the field is known numerically.

gauge one can take advantage of the fact that the solution for the one nucleus case has, besides the gauge condition $A^+ = 0$, also the property^c $A^- = 0$. This is due to the static nature of the current; a x^+ -dependence in the Wilson line (6) would induce a A^- -field. In other words this is a feature of the leading $\ln x$ kinematical regime, where the degrees of freedom in the source are assumed to have a large p^+ , virtuality $\sim p_T^2 \sim Q_s^2$ and therefore a very small p^- . Choosing purely $A^+ = 0$ or $A^- = 0$ as our gauge condition would, however, break the symmetry between the two nuclei in an inconvenient way (see, however¹⁹ for a discussion of the CYM problem in an asymmetric gauge and^{20,21} for a formulation of the problem in a way that is completely asymmetric from the beginning). Fortunately a convenient symmetric axial gauge condition is provided by the temporal, or Fock-Schwinger, gauge in the proper time-rapidity coordinates: $A_\tau = 0$. The other independent linear combination, $A_\eta = -\tau^2 A^\eta = x^+ A^- - x^- A^+$ is zero for the one-nucleus solution, but not in the case of two colliding nuclei. The Schwinger gauge condition in light cone coordinates is $x^+ A^- + x^- A^+ = 0$. In other words, on the $x^+ = 0$ -light cone where there is a current J^- , the gauge condition guarantees that $A^+ = 0$ and the current does not precess, and symmetrically for the other light cone. The effects of the interaction between the two nuclei are now visible only in the gauge field, not the current (at least at the classical level).

^cThis is for the rightmoving nucleus, for the leftmover $A^- = 0$ is the light cone gauge condition and $A^+ = 0$ a property of the particular solution.

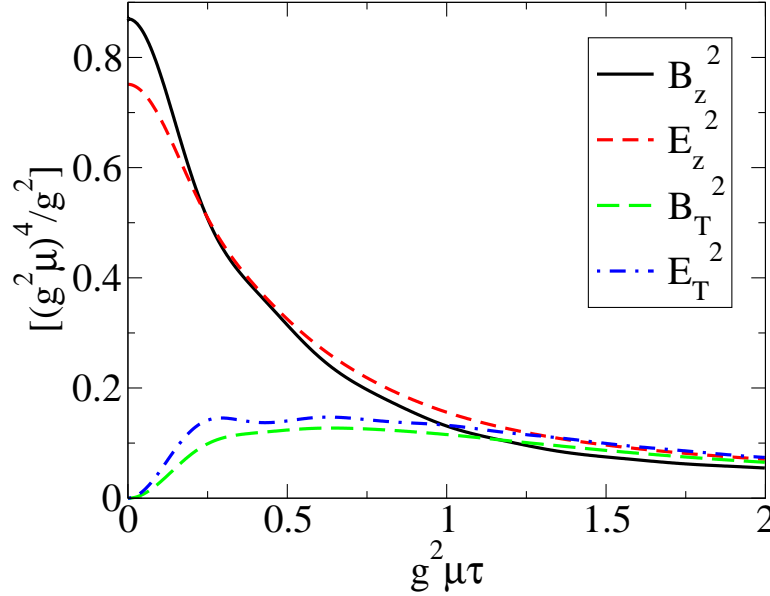


Fig. 2. Components of the gauge field, computed numerically on a 512^2 -lattice with $g^2 \mu R_A = 67.7$.

Inside the future light cone (the spacetime structure is illustrated in Fig. 1) the gauge fields satisfy the equations of motion in vacuum. What is needed is the initial condition for solving these equations. These initial conditions can be obtained by requiring that the fields in the different regions match smoothly on the light cone. In practice this is done by inserting the ansatz

$$A^i = \theta(-x^+) \theta(x^-) A_{(1)}^i + \theta(x^+) \theta(-x^-) A_{(2)}^i + \theta(x^+) \theta(x^-) A_{(3)}^i \quad (10)$$

$$A^\eta = \theta(x^+) \theta(x^-) A_{(3)}^\eta \quad (11)$$

into the equation of motion (1) and requiring that the singular terms arising from the derivatives of the θ -functions cancel. In this way one gets the following initial conditions for the gauge field in the future light cone:

$$A_{(3)}^i|_{\tau=0} = A_{(1)}^i + A_{(2)}^i \quad (12)$$

$$A_{(3)}^\eta|_{\tau=0} = \frac{ig}{2} [A_{(1)}^i, A_{(2)}^i]. \quad (13)$$

The equations of motion with these initial conditions can then be solved either numerically or perturbatively in the weak field limit. We shall turn to these solutions later, but the basic features of the glasma fields can be seen already from the initial conditions.

For a physical interpretation it is useful to calculate the corresponding chromo-electric and -magnetic fields in the usual t, z -coordinate system. The field configurations Eqs. (12) and (13) correspond to vanishing transverse fields and longitudinal

10 *T. Lappi*

components given by

$$E^z = ig[A_{(1)}^i, A_{(2)}^i] \quad (14)$$

$$B^z = ig\epsilon^{ij}[A_{(1)}^i, A_{(2)}^j]. \quad (15)$$

Note that the gauge potential A_μ is a true vector and therefore the longitudinal component A_η corresponds to A_z only at $\eta = 0$. The field strengths \vec{E} and \vec{B} , on the other hand are components of the tensor $F^{\mu\nu}$ and Eqs. (14) and (15) are true for all η . Solving the equations of motion forward in time then generates also transverse components for the fields within a time $\sim 1/Q_s$. A plot of the transverse and longitudinal color field strengths as a function of τ from a numerical calculation is shown in Fig. 2.

The color fields of the two individual nuclei are transverse electric and magnetic fields on the light cone. Why then are the glasma fields in the region between the two nuclei longitudinal along the beam axis? One way of understanding these field configurations is the following. Let us work still in the $A_\tau = 0$ gauge, so that each nucleus, when going past a point on the beam axis with no gauge field before the collision, leaves behind it a pure gauge field (see Fig. 1). One can define an effective chromoelectric and chromomagnetic charge density by separating the nonlinear parts of the vacuum Gauss law and Bianchi identities

$$[D_i, E^i] = 0 \quad \text{and} \quad [D_i, B^i] = 0 \quad (16)$$

as

$$\partial_i E^i = \rho_e = ig[A^i, E^i] \quad \text{and} \quad \partial_i B^i = \rho_m = ig[A^i, B^i]. \quad (17)$$

Now we can interpret the interaction of the WW chromoelectric and -magnetic fields of the nucleus on the x^+ -light cone with the pure gauge field left behind by the other nucleus as an effective chromoelectric and -magnetic charge density left behind on the light cone. An exactly opposite charge density is left behind on the other sheet, leading to a longitudinal chromoelectric and -magnetic field between the sheets. This structure is illustrated in Fig. 3. This description is very similar in spirit to the original suggestions for a string based description of a hadronic collisions. These string picture had only sources of electric charge²². When these longitudinal field configurations are actually derived from the QCD equations of motion also a magnetic field naturally appears.

It is interesting to note the structure of the energy momentum tensor $T_{\mu\nu} = \frac{1}{4}g_{\mu\nu}F^{\alpha\beta}F_{\alpha\beta} - F_\mu^\alpha F_{\nu\alpha}$ for this initial condition. It is diagonal and, as always in gauge theory at the classical level, traceless: $T_{\mu\nu} = \frac{1}{2}(E_z^2 + B_z^2) \times \text{diag}(1, -1, -1, 1)$. This can be compared to the standard form for a system with an anisotropy in the z -direction: $T_{\mu\nu} = \text{diag}(\epsilon, -p_\perp, -p_\perp, -p_L)$, where ϵ is the energy density and p_\perp and p_L are the transverse and longitudinal pressures. We see that the initial field configuration has *negative* “longitudinal pressure”. The configuration that is the starting point for studies of isotropization by plasma instabilities, where the diagonal elements of $T_{\mu\nu}$ at $\eta = 0$ are $(\epsilon, -\epsilon/2, -\epsilon/2, 0)$, is only reached at times

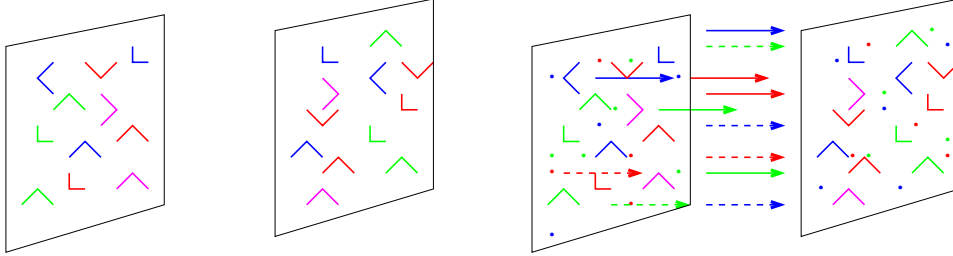


Fig. 3. The WW fields of the two nuclei before and after the collision. Before the collision there are only transverse fields on the sheets. After the collision the interaction of these fields with the pure gauge field of the other nucleus leaves behind an effective electric and magnetic charge density (the dots on the figure) on the sheet, and a longitudinal electric and magnetic field between these effective charges.

$\tau \gtrsim 1/Q_s$ when the classical fields start to behave linearly due to the expansion of the system.

The glasma field configurations depend on the transverse coordinate at the length scale $1/Q_s$, which corresponds to the typical transverse momentum of the gluons being $\sim Q_s$. The same scale is also in general the correlation length of the system, and will as such determine the strength of multigluon correlations as we shall see in Sec. 6. This leads to the lifetime of the purely longitudinal field configuration also being $\sim 1/Q_s$. For the bulk of particle production there is therefore no clear separation of timescales that would justify treating the field as constant in time and space, no matter how appealing this approximation might be for those used to low energy string phenomenology. The difference between the glasma and the Lund string model is that conceptually the transverse scale of the problem is a semi-hard scale Q_s , not the confinement scale Λ_{QCD} . Note also that the initial fields being longitudinal along the beam axis direction is in no contradiction with the lowest order perturbative description of the process as $gg \rightarrow g$ scattering, because the longitudinal (with respect to the beam axis) fields are perpendicular to the momentum of the gluon being produced. The initial polarization state of this gluon is, however, a very particular one.

The field inside the future light cone can then be computed either numerically^{23,24,25} or analytically in different approximations (see e.g.¹⁹ for recent work). The obtained result is then averaged over the configurations of the sources J^μ with a distribution $W_y[J^\mu]$ that includes the nonperturbative knowledge of the large x degrees of freedom. The resulting fields are then decomposed into Fourier modes to get the gluon spectrum. This is the method that we will refer to as Classical Yang-Mills (CYM) calculations. Note that the average over configurations is a classical average over a probabilistic distribution. This is guaranteed by a theorem^{26,27} ensuring the factorization of leading logarithmic corrections to gluon production into the quantum evolution of $W_y[J^\mu]$, analogously to the way leading logarithms of Q^2 are factorized into DGLAP-evolved parton distribution functions.

In the limit when either one or both of the color sources are dilute (the “pp” and “pA” cases), the CYM calculation can be done analytically and reduces to a factorized form in terms of a convolution of unintegrated parton distributions that can include saturation effects:

$$\frac{dN}{d^2\mathbf{p}_T dy} = \frac{1}{\alpha_s} \frac{1}{\mathbf{p}_T^2} \int \frac{d^2\mathbf{k}_T}{(2\pi)^2} \varphi_y(\mathbf{k}_T) \varphi_y(\mathbf{p}_T - \mathbf{k}_T). \quad (18)$$

Although this approach (known as “KLN” after the authors of ^{28,29}, see⁶ for the original work) is not strictly valid for the collision of two dense systems, it does have the advantage of offering some analytical insight and making it easier to incorporate large- x ingredients into the calculation. We will discuss these calculations of the gluon spectrum in more detail in Sec. 4.

2.3. Factorization

In the previous discussion we did not specify the probability distribution of the color charge densities more precisely, besides mentioning the MV model as a phenomenological approximation. The color charge distribution $W_y[\rho]$ includes nonperturbative information about the large- x part of the nuclear wavefunction, i.e. the valence degrees of freedom boosted from the rest frame of the nucleus. Thus the probability distribution cannot be computed from first principles in weak coupling. Nevertheless, by considering quantum corrections to high energy scattering, it is possible to derive a *renormalization group* equation that is known by the acronym JIMWLK^{7,8} (pronounced as “gym-walk”). The JIMWLK equation describes the dependence of the probability distribution $W_y[\rho]$ on y , the rapidity (or, equivalently in the leading log high energy kinematics that we are working in, on $\ln 1/x$). In a mean-field approximation valid in the large N_c -limit the JIMWLK evolution of the correlation function of two Wilson lines reduces to the BK^{30,31} equation.

The role of $W_y[\rho]$ is analogous to the conventional parton distribution function; it is a nonperturbative quantity whose dependence on one of the kinematical variables of the process is described by a weak coupling renormalization group equation. In the case of parton distributions, the renormalization group equations are the DGLAP ones, and they describe evolution in Q^2 . In the case of DGLAP one is dealing with a dilute system, where the appropriate degrees of freedom are individual partons with a definite momentum, whereas in the case of the CGC the good degrees of freedom are color charges resulting from interactions of many partons. The distributions $W_y[\rho]$ are similar to parton distributions in the sense that they are not (complex) wavefunctions but (at least loosely speaking) real probability distributions. This is guaranteed by *factorization theorems* stating that there is no interference between the dynamics of the hadrons or nuclei at large x (JIMWLK; or BFKL) or at small Q^2 (DGLAP) and the process one is studying. Factorization can be understood as a statement that one has found the right set of degrees of freedom in which one can compute physical observables from only the diagonal elements of the density matrix of the incoming nuclei.

In our nonlinear high-energy context the JIMWLK equation was derived in the context of deep inelastic scattering off a nuclear target. In the case of particle production in the glasma, it was shown more recently^{32,26} that when one computes the NLO quantum corrections to a given observable in the Glasma, all the leading logarithmic divergences can be absorbed into the RG evolution of the sources with the same Hamiltonian that was derived by considering only the DIS process. The underlying physical reason for factorization is that this fluctuation with a large k^+ requires such a long interval in x^+ to radiated that it must be produced well before and independently of the interaction with the other (left moving and thus localized in x^+) source.

In the case of the spectrum of gluons produced in a high energy collision the leading log divergence can be written as two JIMWLK Hamiltonians, one for each nucleus, acting on the expression for the leading order spectrum. This same Hamiltonian describes the RG evolution of the source distributions $W_y[\rho]$. It is most naturally expressed as

$$\mathcal{H} \equiv \frac{1}{2} \int d^2\mathbf{x}_T d^2\mathbf{y}_T D_a(\mathbf{x}_T) \eta^{ab}(\mathbf{x}_T, \mathbf{y}_T) D_b(\mathbf{y}_T) \quad (19)$$

in terms of Lie derivatives $D_a(\mathbf{x}_T)$ operating on the Wilson lines, Eq. (6), constructed from the source color charge densities. The kernel in Eq. (19) is a function of these same Wilson lines:

$$\eta^{ab}(\mathbf{x}_T, \mathbf{y}_T) = \frac{1}{\pi} \int d^2\mathbf{u}_T \frac{(\mathbf{x}_T - \mathbf{u}_T) \cdot (\mathbf{y}_T - \mathbf{u}_T)}{(\mathbf{x}_T - \mathbf{u}_T)^2 (\mathbf{y}_T - \mathbf{u}_T)^2} \left[U(\mathbf{x}_T) U^\dagger(\mathbf{y}_T) - U(\mathbf{x}_T) U^\dagger(\mathbf{u}_T) - U(\mathbf{u}_T) U^\dagger(\mathbf{y}_T) + 1 \right]^{ab}. \quad (20)$$

The fact that no other divergent terms appear is the proof of factorization; this is the central result of Ref.²⁶.

3. Nuclear wavefunction

3.1. Deep inelastic scattering

The most direct probe of the nuclear wavefunctions would be to perform nuclear deep inelastic scattering experiments at high energy such as at the Electron-Ion Collider (EIC)³³ or a Large Hadron-electron Collider (LHeC)³⁴. In the meantime one has to rely on the few existing, relatively low energy, measurements and theoretical extrapolations from proton data from HERA. For a review of the existing understanding of nuclear shadowing we refer the reader to the review by Armesto³⁵.

It is useful to think of deep inelastic scattering at small x in the dipole picture^{37,38}, where the process is viewed as a virtual quark fluctuating into a color dipole, which then probes the wavefunction of the target (see Fig. 4).

In the dipole model one factorizes the total cross section into the probability for the virtual photon to fluctuate into a $q\bar{q}$ pair (a color dipole) and the cross section

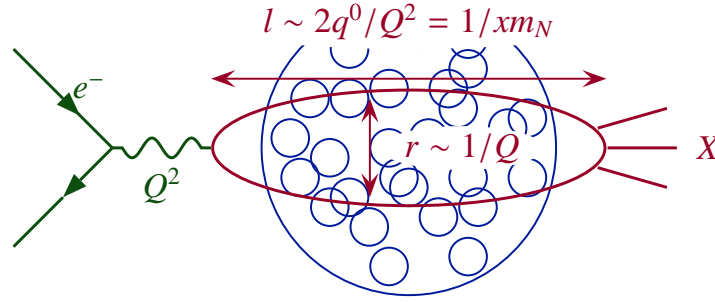


Fig. 4. In the dipole frame the incoming virtual photon splits into a quark-antiquark dipole of transverse size r_T , which then interacts with the target with the dipole cross section $\hat{\sigma}$.

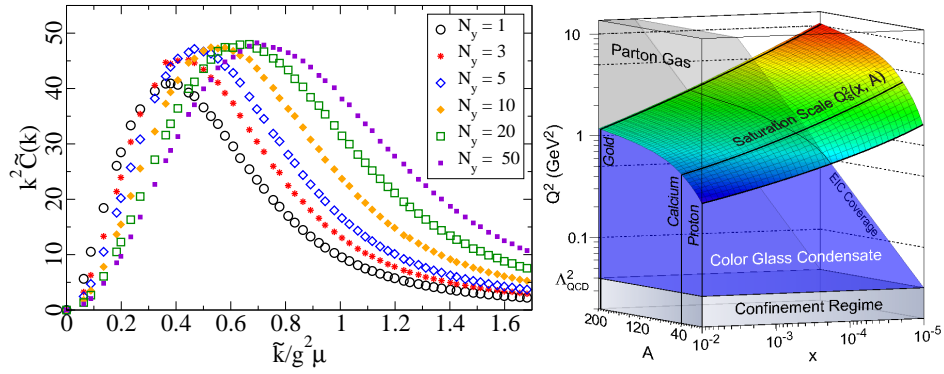


Fig. 5. Left: Wilson line correlator multiplied by k_T^2 in the MV model, with different discretizations of the longitudinal coordinate¹⁸ (see Eq. (25) below). Reading off the maximum of these curves and defining the corresponding k_T as Q_s is one possible way to relate the parameters of the MV model to Q_s . Right: estimate of the numerical value of the saturation scale, based on a fit to HERA data and a Woods-Saxon parametrization of the nuclear geometry^{36,16}.

of the dipole scattering with the target^d. The total cross section can be written as 41,38,

$$\sigma_{T,L}(x, Q^2) = \int d^2\mathbf{r}_T \int_0^1 dz |\psi_{T,L}(z, \mathbf{r}_T)|^2 \sigma_{\text{dip}}(x, Q^2, \mathbf{r}_T). \quad (21)$$

Here the *photon wave function* $\psi_{T,L}(z, \mathbf{r}_T)$ gives the probability for the virtual photon (T and L stand for, respectively, transverse and longitudinal polarizations of the photon) to split into a color dipole of transverse size \mathbf{r}_T . The wave function $\psi_{T,L}(z, \mathbf{r}_T)$ includes the known QED part of the reaction and is known analytically^e.

^dThere are some tricky issues related to the Lorentz frame in which one should view the scattering process in the dipole model, see e.g. the discussion in ^{39,40}.

^eTo leading order in α_{em} , which is quite sufficient in this context.

The exact expressions can be found in e.g. ⁴¹. In the classical field approximation the dipole cross section can be expressed in terms of the Wilson lines $U(\mathbf{x}_T)$ appearing in Eq. (6) as^{30,42,43}

$$\begin{aligned}\sigma_{\text{dip}}(\mathbf{r}_T) &= \frac{2}{N_c} \int d^2\mathbf{b}_T \text{Tr} \left\langle 1 - U^\dagger(\mathbf{b}_T + \frac{1}{2}\mathbf{r}_T) U(\mathbf{b}_T - \frac{1}{2}\mathbf{r}_T) \right\rangle \\ &= 2 \int d^2\mathbf{b}_T \mathcal{N}(\mathbf{b}_T, \mathbf{r}_T),\end{aligned}\quad (22)$$

where we have denoted the imaginary (and dominant at high energy) part of the dipole-target scattering amplitude with $\mathcal{N}(\mathbf{b}_T, \mathbf{r}_T)$. Equation (22) provides a direct and explicit connection with between DIS observables and the classical field description of the initial color fields in a nucleus-nucleus collision. For small dipoles the scattering amplitude is proportional to \mathbf{r}_T^2 , whereas for a large one it approaches the unitarity limit $\mathcal{N} = 1$. The saturation scale Q_s is defined as the characteristic momentum scale separating these two regimes. Fourier-transforming the Wilson line correlator w.r.t. \mathbf{r}_T into momentum space Q_s could be defined as the k_T corresponding to the maximum of the function $k_T^2 \mathcal{N}(\mathbf{b}_T, \mathbf{k}_T)$. In coordinate space one can define it from the value of \mathbf{r}_T when the scattering amplitude reaches some characteristic value. For example one can choose to define $Q_s(\mathbf{b}_T)$ by the relation⁴⁴ $\mathcal{N}(\mathbf{b}_T, r_T = \sqrt{2}/Q_s) = 1 - e^{-1/2}$ or by¹⁶ $\mathcal{N}(\mathbf{b}_T, r_T = 1/Q_s) = 1 - e^{-1/4}$. Several other constants in lieu of $1 - e^{-1/2}$ or $1 - e^{-1/4}$ are used by different authors, leading to slightly different numerical values. The three cited above have the advantage agreeing with the convention used in the well-known ‘‘GBW’’ fit^{41,45} to HERA data which is discussed below (see Eq. (24)). The momentum space Wilson line correlator in the MV model is shown in Fig. 5 (left).

3.2. Proton-nucleus collisions

Another avenue to access properties of the nuclear wavefunction is to study proton-nucleus collisions and compare them with nucleus-nucleus ones. Here the idea is to treat the proton as dilute probe scattering off the CGC of the nucleus. Among CGC theorists it is a common terminology to denote generally the (formal) dilute-dense limit of scattering by ‘‘pA’’^{47,48,49,50}; many of the results are equally valid for forward scattering in AA collisions⁵¹. Deuteron-nucleus (falling into the same dense-dilute category) collisions at RHIC have turned out to be a very powerful tool to access properties of the small x nuclear wavefunction. Indeed the suppression of high p_T hadron production in pA collisions at forward rapidities observed by the BRAHMS collaboration⁵² have been considered as one of the clearest direct experimental signals from RHIC favoring gluon saturation. Much of the theoretical context and the earlier phenomenological applications have been extensively presented in the review by Jalilian-Marian and Kovchegov⁵³, and we shall here discuss them only briefly. More recently the focus in pA collisions as well as nucleus-nucleus ones has been on azimuthal and rapidity correlations; we shall return to these towards

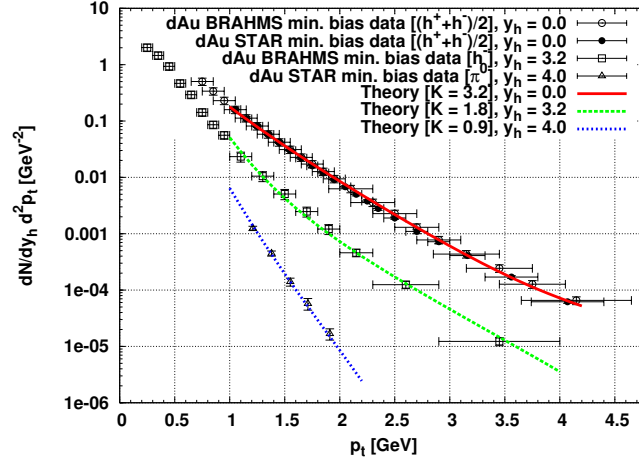


Fig. 6. Hard particle spectra in dAu collisions using the DHJ parametrization of the dipole cross sections⁴⁶.

the end of this section.

In pA-collisions the particularly interesting kinematical regime is in the forward rapidity region (proton fragmentation region, i.e. small x in the nucleus and large x in the proton), where the nuclear saturation scale is large and the proton (deuteron in practice) is a dilute probe. Here one is typically dealing with particle production at large transverse momenta compared to the intrinsic \mathbf{k}_T in the proton wavefunction, and it is necessary to resum the large DGLAP logarithms on the proton side. One must also take into account both the quark and gluon degrees of freedom from the proton, whose scattering off the CGC target depends on the Wilson line correlator in different representations. The single inclusive hadron spectrum can be written as⁵⁴

$$\frac{d\sigma^{pA \rightarrow hX}}{dy d^2\mathbf{p}_T d^2\mathbf{b}_T} = \frac{1}{(2\pi)^2} \int_{x_F}^1 dx_p \frac{x_p}{f_f} \left\{ f_{q/p}(x_p, Q^2) \mathcal{N}_F \left[\frac{x_p}{x_F} \mathbf{p}_T, \mathbf{b}_T \right] D_{h/q} \left(\frac{x_F}{x_p} \right) + f_{g/p}(x_p, Q^2) \mathcal{N}_A \left[\frac{x_p}{x_F} \mathbf{p}_T, \mathbf{b}_T \right] D_{h/g} \left(\frac{x_F}{x_p} \right) \right\} \quad (23)$$

Here $f_{q,g/p}$ are the gluon distribution functions in the proton and $D_{h/q,g}$ the fragmentation functions of quarks and gluons into the hadron h . The Wilson line correlators $\mathcal{N}_{F,A}$ (as in Eq. (22)) in the fundamental and adjoint representations have to be evaluated in at the rapidity scale (x the nuclear wavefunction corresponding to the produced hadron). A similar approximation for only the gluonic contribution can be derived from the k_T -factorized formulation discussed in Sec. 4 and has also often been used in applications to the spectrum in pA collisions. A comparison of Eq. (23) using a certain parametrization (“DHJ”⁴⁶) with experimental data is shown in Fig. 6. Computing the spectrum in pA collisions at different rapidities

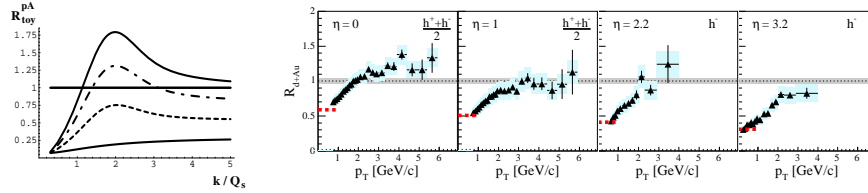


Fig. 7. Left: nuclear modification factor R_{pA} from BRAHMS⁵². Right: qualitative prediction of the evolution of R_{pA} from a CGC calculation⁵⁶.

enables one to almost directly see the effects of high energy evolution in the nuclear wavefunction on the Wilson line correlators $\mathcal{N}_{F,A}$. At the starting scale of the evolution one generically expects a ‘‘Cronin’’ enhancement in pA compared to pp collisions. This, as can explicitly be seen e.g. in the M.V. model, is due to the saturation in the nuclear wavefunction that suppresses the gluon distribution below Q_s^A and causes an enhancement above Q_s (the ‘‘Cronin peak’’). The effect of high energy evolution is to wash this peak away^{55,56,57}, which is seen in the data at more forward rapidities, as shown in Fig. 7.

A more recent area of activity are two-particle correlations in dAu collisions^{58,59}. The baseline comparison is the structure observed in proton-proton collisions, where high p_T particles typically originate from back-to-back jets. The azimuthal structure of the two particle correlation is thus a rather narrow peak on the away-side resulting from the fragmentation of the original jet into a narrow cone. The expectation from the CGC picture is essentially that of an increased collectivity in the correlation, signaling itself as a flattening and broadening of the away-side peak^{60,61}. This feature should become more prominent as the kinematics of the two particles move towards small x_A (when the saturation scale becomes larger) and should be very sensitive to the relation between the trigger p_T ’s and Q_s . A result of a particular calculation⁶¹ is shown in Fig. 8, together from recent experimental data from STAR⁵⁹.

3.3. Dipole cross section parametrizations

By now there is a wide variety of saturation-based parametrizations of the dipole cross section, mostly fitted to HERA data. While the aim here is not to give a comprehensive listing, let us mention a few. One of the problems of practical parametrizations is that calculations of DIS observables (as in Eq. (21)) use the dipole cross section as a function of \mathbf{r}_T , the size of the dipole, what one needs to compute particle production in pA collisions (as in Eq. (23)) is the Fourier-transform. Although it is not strictly speaking formally required, one would prefer to have a parametrization that is positive definite in both position and momentum space, while retaining some other general features required in different limits. It has turned out to be a surprisingly difficult mathematical problem⁶² to find such a parametrization. The result of difficulty has been that many authors prefer to use

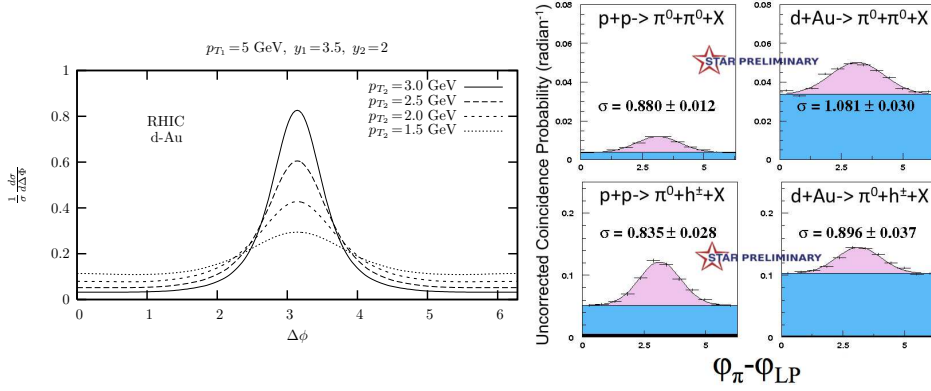


Fig. 8. Prediction for broadening of the two-particle correlation function in deuteron-nucleus collisions from Ref.⁶¹. Right: corresponding data from the STAR collaboration⁵⁹.

different parametrizations for DIS and for pA studies, thus reducing the predictive power of the respective calculations.

The early and widely used “GBW”^{41,45} dipole cross section is a Gaussian in \mathbf{r}_T , and consequently also in \mathbf{k}_T :

$$\sigma_{\text{dip}}(x, Q^2, \mathbf{r}_T) = \sigma_0(1 - e^{-\mathbf{r}_T^2 Q_s^2(x)/4}), \quad (24)$$

with $Q_s^2(x) \sim x^{-\lambda}$ with $\lambda \approx 0.3$ resulting from the fit to HERA data. This formula features the idea of parton saturation very clearly. The exponential decrease at high momenta is, however, not very physical. At very large \mathbf{k}_T one would expect $\sigma_{\text{dip}}(\mathbf{k}_T)$ to behave as $\sim 1/\mathbf{k}_T^4$ in order to recover a DGLAP-like increase of the gluon distribution at high momenta: $xG(x, Q^2) \sim \ln Q^2$; one of the attractive features of the MV model is precisely that it results in this behavior. At somewhat smaller momenta, $k_T \gtrsim Q_s$ BK/JIMWLK evolution predicts a different power law $\sigma_{\text{dip}}(\mathbf{k}_T) \sim k_T^{-2(1+\gamma)}$ with an anomalous dimension $\gamma \approx 0.6$. In the “BKW” parametrization⁶³ the large k_T behavior is modified by replacing the exponent $\mathbf{r}_T^2 Q_s^2$ by $\mathbf{r}_T^2 xG(x, 1/\mathbf{r}_T^2)$, where $xG(x, 1/\mathbf{r}_T^2)$ is a DGLAP-evolved gluon distribution evaluated at the scale $\mu_0^2 + 4/\mathbf{r}_T^2$. This brings the high- k_T limit closer to a DGLAP-like behavior, but applying the DGLAP-evolved distribution around the saturation scale is not without problems; in particular it turns out that the best fit to data is given by a gluon distribution which *decreases* towards smaller x at the initial scale μ_0^2 . A dipole cross section that reproduces, instead of DGLAP, the behavior of BK evolution in the extended scaling region $k_T \gtrsim Q_s$ is given by the “IIM”⁶⁴ parametrization.

Another simplification in Eq. (24) is the dependence on the impact parameter \mathbf{b}_T . The impact parameter profile of the dipole scattering amplitude can be directly measured from the t -distribution of diffractive events; experiments are consistent with a Gaussian in \mathbf{b}_T (implying an exponential dependence on t). In

Eq. (24) the impact parameter dependence $T(\mathbf{b}_T)$ has been factorized from the \mathbf{r}_T -dependence, which reduced it in the total cross section into a constant proton area $\sigma_0 = \int d^2\mathbf{b}_T T(\mathbf{b}_T)$. The problematic aspect of this factorization is that the unitarity limit of the scattering amplitude is only approached at $b = 0$ (see more detailed discussion in Ref.⁶⁵). Two parametrizations attempting to treat the b -dependence more consistently, either in a DGLAP-improved approach or parametrizing features of BK evolution are provided by the IPSat (also “KT”³⁶) and bCGC models⁴⁴. In these parametrizations the saturation scale is impact parameter dependent.

The “KKT”⁶⁶ and “DHJ”⁴⁶ parametrizations, also including a BK-like anomalous dimension, have been used in pA collisions, but not fitted to DIS data. There are also by now several numerical evaluations^{67,51} of the BK equations numerically both with fixed and running coupling. The initial condition of the evolution can then be used to fit experimental data and produce a parametrization⁶⁸ for use in other contexts. A recent application of a direct solution of the BK equation to hadron spectra in pA collisions can be found in Ref.⁶⁹.

4. Bulk gluon production in nucleus-nucleus collisions

Let us now turn back to the case of the collision of two dense systems. The first question to understand are the properties, such as entropy or energy density, of the initial stage in a heavy ion collision in the CGC framework. As we have discussed, the initial stage of the collision system at central rapidities is, to a first approximation, gluonic and boost invariant. It is therefore far from chemical and thermal equilibrium (in particular anisotropic, with much larger transverse than longitudinal momenta). The thermalization of this gluonic system towards a quark-gluon plasma is not quantitatively understood, in spite of a lot of recent work on exploring the instabilities that could dominate this stage⁷⁰.

To make a more direct connection to phenomenology one must thus at this stage try to shortcut the thermalization stage by replacing it with a more schematic relation between the initial gluon spectrum and the later stage evolution of the system. One simple version of this relation, based on experimental observation, goes by the name of “parton-hadron duality”, stating that the final state hadron multiplicity is proportional to that of the initial partons. A second way of estimating the relation is based on the argument that the particle multiplicity cannot decrease during the thermalization process, due to the second law of thermodynamics and the fact that the entropy is essentially proportional to the particle density. On the other hand the energy per unit of rapidity can only decrease (due to $p dV$ work, i.e. flow of energy towards the fragmentation region) during the time evolution. Thus one can to some extent estimate the relation between the initial gluon multiplicity and energy density and the final (charged hadron) multiplicity and transverse energy. In particular it seems reasonable to assume that the dependences of both on centrality, collision energy and rapidity would be similar.

4.1. *Calculating the initial gluon multiplicity*

It is thus of direct phenomenological interest to try to calculate the initial gluon multiplicity in the CGC framework with, as much as possible, input values of the parameters determined from independent observables, in particular from DIS or pA data. As already mentioned in Sec. 2, there are two major ways of doing this. One is to directly solve the classical Yang-Mills equations numerically (“CYM”, the other is to use a k_T -factorized approximation (“KLN”) in a situation where it strictly speaking is not valid. The results from both approaches for the integrated gluon multiplicity, if not for the spectrum as a function of momentum, turn out to be very similar. This can mostly be understood by dimensional analysis. Gluon production in a central collision, at midrapidity, is a one scale problem with Q_s as the only relevant dimensionful scale. The gluon density must therefore be $dN/dy d^2\mathbf{x}_T \sim Q_s^2$. In a noncentral collision or away from midrapidity the saturation scales of the two nuclei are different, but the generic result in both the CYM and KLN calculations is that $dN/dy d^2\mathbf{x}_T \sim Q_{s\min}^2$, where $Q_{s\min}^2$ is the smaller of the two saturation scales. Thus the dependence of the integrated multiplicity on centrality is determined by the impact parameter dependence of the saturation scale, and the dependence on rapidity and collision energy by its x -dependence. The next natural observable to look at would be the energy density, which probes an integral of the gluon spectrum weighted by an extra power of p_T . This is more sensitive to the large momentum part of the spectrum, which would typically behave as $1/p_T^4$ (as resulting from the expected $1/k_T^2$ -behavior of the unintegrated gluon distribution) in both cases. The actual gluon spectrum from the CYM and KLN calculations can be very different especially for $k_T \lesssim Q_s$, but it is difficult to get an experimental handle on the shape of the spectrum.

Typically in KLN calculations, if the value of Q_s is fixed by an external input, the normalization of the result is adjusted by hand to a reference point in the data. In particular, in the k_T -factorized approximation in the cases where one can derive it from the CGC framework the integrated gluon spectrum is not IR finite; although the divergence is only logarithmic instead of a power law due to saturation. In practical calculations one must thus add an additional regulating prescription with the corresponding adjustment to the normalization. This adjustment of the normalization is not possible in the CYM calculation, where the only parameter one has is essentially Q_s , which determines both the number and the typical transverse momentum of the gluons produced. Thus in the CYM framework it has turned out to be more realistic to make a genuine prediction for the normalization of the spectrum based only on the value of Q_s obtained from HERA data; we will discuss this estimate below. Due to the relative simplicity of the analytic k_T -factorized approximation, on the other hand, it is easier to incorporate more detailed features of the transverse coordinate or rapidity dependence.

Most of the original CYM calculations were done using the MV model, treating the color charge density $g^2\mu$ as a free parameter to be adjusted to RHIC data. We

shall here follow the approach of Ref.¹⁸ to take these results and transform them *a posteriori* to parameter-free RHIC postdictions using the numerically determined relation between $g^2\mu$ and Q_s and values of Q_s extracted from HERA fits.

Let us first recall the results of the numerical CYM calculations of the gluon spectrum in heavy ion collisions^{71,23,72,24,25,73}. We shall not discuss the numerical procedure here; a recent review is given in⁷⁴. In order to compare the results we must, however, comment on one aspect of the numerical implementation of the MV model. In the numerical implementation of the MV model the Wilson lines (6) are constructed as

$$U(\mathbf{x}_T) = \prod_{k=1}^{N_y} \exp \left\{ -ig \frac{\rho_k^{1,2}(\mathbf{x}_T)}{\nabla_T^2 + m^2} \right\}, \quad (25)$$

where the color charges are Gaussian variables with the variance

$$\langle \rho_k^a(\mathbf{x}_T) \rho_l^b(\mathbf{y}_T) \rangle = \delta^{ab} \delta^{kl} \delta^2(\mathbf{x}_T - \mathbf{y}_T) \frac{g^2 \mu_A^2}{N_y}. \quad (26)$$

The indices $k, l = 1 \dots N_y$ represent a discretization of the longitudinal direction into N_y small steps; the continuum limit corresponding to Eq. (6) is achieved for $N_y \rightarrow \infty$ at constant $g^2\mu_A$. Some kind of infrared regulator is needed in order to invert the Laplacian operator ∇_T^2 ; it can be regularized by the scale m in Eq. (25). As pointed out in Ref.¹⁸ (see also¹⁷), the relation between the parameter $g^2\mu$ of the model and the physical length scale Q_s , the correlation length of the Wilson lines in the transverse plane, depends on N_y . The conceptual picture CGC framework is that of a Wilson line built up from infinitesimal steps in rapidity, i.e. $N_y \rightarrow \infty$. The early numerical implementations, on the other hand, used $N_y = 1$ for simplicity. When expressed in terms of the physical length scale Q_s the results depend very little on the way the Wilson lines were constructed. However, when comparing the results of the numerical calculations to phenomenology and using values of Q_s extracted independently one must take care to use the correct relation between Q_s and $g^2\mu$. As shown in¹⁸, the relation corresponding to $m \rightarrow 0, N_y = 1$; i.e. the prescription used in the numerical CYM calculations, is $Q_s \approx 0.57g^2\mu$.

With this conversion between Q_s and $g^2\mu$ explicitly stated let us then proceed to the result of the numerical CYM computations. The energy and multiplicity per unit rapidity can be parametrized as

$$\frac{dN}{d\eta} = \frac{(g^2\mu)^2 \pi R_A^2}{g^2} f_N \quad (27)$$

$$\frac{dE_T}{d\eta} = \frac{(g^2\mu)^3 \pi R_A^2}{g^2} f_E. \quad (28)$$

The numerical result (see in particular Refs.^{24,25}) is $f_E \approx 0.25$ and $f_N \approx 0.3$. We can also recast this expression in terms of the the ‘‘liberation coefficient’’ c , introduced by A. Mueller^{75,76,77}, The liberation coefficient is defined by writing

22 *T. Lappi*

the produced gluon multiplicity as

$$\frac{dN}{d^2\mathbf{x}_T dy} = c \frac{C_F Q_s^2}{2\pi^2 \alpha_s}. \quad (29)$$

With Eq. (27) this leads to

$$c = \frac{\pi f_N}{2C_F} \left(\frac{g^2 \mu}{Q_s} \right)^2. \quad (30)$$

The original expectation was that c should be of order unity^{78,77}. The analytical calculation by Y. Kovchegov⁷⁶ gave the estimate $c \approx 2 \ln 2 \approx 1.4$. With $f_N = 0.2$ in Eq. (27) and $Q_s/g^2 \mu \approx 0.57$ we see that the CYM result for the liberation coefficient is $c \approx 1.1$. A demonstration of the independence of this number on the details of the Wilson line correlator can be made by replacing the MV model distribution by another one. For example, if the Wilson lines are constructed explicitly to correspond to the IPsat^{36,16} (Kowalski-Teaney) or bCGC^(64,16) parametrization of HERA data, the result for the liberation coefficient c is the same as in the MV model across the whole energy range from RHIC to the LHC⁷⁹. This is the result in spite of the very different forms of the gluon spectra at high k_T in the models.

The estimates for the values of Q_s based on HERA data, nuclear geometry and attempts to fit the limited available nuclear DIS data^{80,81} vary somewhat, especially due to the degeneracy between the proton size and the value of Q_s in the HERA fits; see e.g.¹⁸ for a comparison of the numerical values. We take here the IPsat estimate¹⁶ that removes this interplay by fixing the size of the proton from diffractive data, where it can be directly measured. The estimate amounts to $Q_s \approx 1.2$ GeV for an average central RHIC collision at midrapidity^{16,18}. As noted previously, this corresponds to the MV model parameter $g^2 \mu \approx 2.1$ GeV (at $N_y = 1$) in the CYM simulations. Plugging this number into Eq. (27) leads to the estimate of $\frac{dN}{dy} \approx 1100$ gluons in the initial stage of a central gold-gold collision at midrapidity at RHIC. This is very close to the observed final total (charged+neutral) particle multiplicity. In other words, recalling our discussion earlier in this section, this points towards a very rapid thermalization that practically conserves particle number, and leaves very little room for higher order effects to increase the multiplicity during the thermalization stage.

4.2. Energy and rapidity dependence

As we discussed, the gluon multiplicity is, across different parametrizations to a very good approximation proportional to $\pi R_A^2 Q_s^2 / \alpha_s$. Thus the predictions for LHC collisions depend mostly on the energy dependence of Q_s . On this front there is perhaps more uncertainty than is generally acknowledged, the estimates for $\lambda = d \ln Q_s^2 / d \ln 1/x$ varying between $\lambda = 0.29$ ⁴¹ and $\lambda = 0.18$ ⁴⁴ in fixed coupling fits to HERA data, with a running coupling solution of the BK equation giving something in between these values⁸². This dominates the uncertainty in predictions for the LHC multiplicity (see Fig. 9).

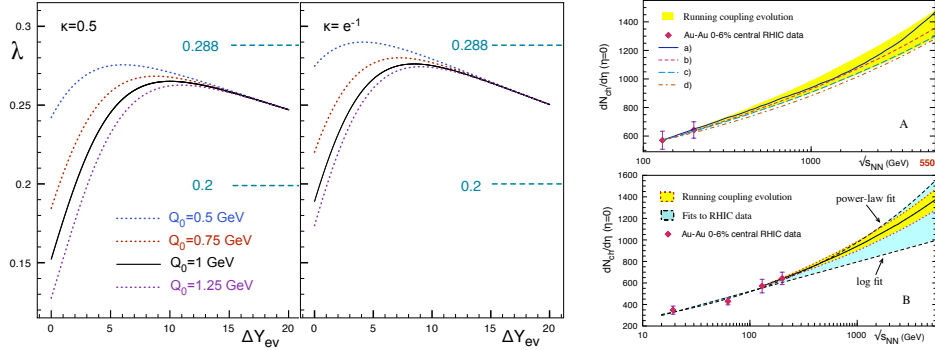


Fig. 9. Predictions for the evolution speed from the running coupling BK equation and the subsequent gluon multiplicity extrapolated to LHC energies from Ref.⁸².

The RHIC collision energy is still too slow to clearly see any saturation effects in the rapidity dependence of the multiplicity around $y = 0$. A simple estimate for the effects of large x physics, such as momentum conservation, is to consider the typical $(1-x)^4$ -dependence of gluon distributions at large x . Inserting $x = e^{\pm y} \langle p_{\perp} \rangle / \sqrt{s}$ leads to the estimate $\Delta y \sim \sqrt{8\sqrt{s}/\langle p_{\perp} \rangle}$ for the rapidity scale at which the large x effects contribute to the rapidity distribution around $y = 0$. This means that the $(1-x)^4$ -behavior starts to dominate the rapidity dependence of the multiplicity around midrapidity at a scale of $\Delta y \sim 4$ RHIC and $\Delta y \sim 19$ at the LHC. Note also that the large x contribution is an effect of order 1 at this scale, whereas small x evolution can be expected to give a much smaller effect⁷³ at a rapidity scale $\Delta y \sim 1/\alpha_s \sim 3$. Only at the LHC the large x effects will be mostly absent around midrapidity and one has a good possibility of seeing a clear signal of CGC effects in the rapidity dependence of the multiplicity.

5. Transverse geometry

Relativistic heavy ion collisions can take place with any impact parameter, from very peripheral ones that should look like simple nucleon-nucleon collisions to central ones that actually produce a system of the size of the colliding nuclei. Experimentally this provides a tool to study quantities as a function of the system size, assuming that one is able to detect the centrality. The impact parameter not being a measurable quantity *per se*, there are basically two methods used to extract the collision centrality in experiments. One is to measure the noninteracting spectator nucleons in the zero-degree calorimeters (ZDC) and the other to make a simple assumption on the dependence of the charged multiplicity in some part of the detector on the size of the system. This is usually done via a Monte Carlo Glauber calculation, which enables one to compute the distributions of N_{part} and N_{coll} (the numbers of participant nucleons and binary nucleon-nucleon collisions) for a fixed impact parameter; assuming that the individual nucleon-nucleon colli-

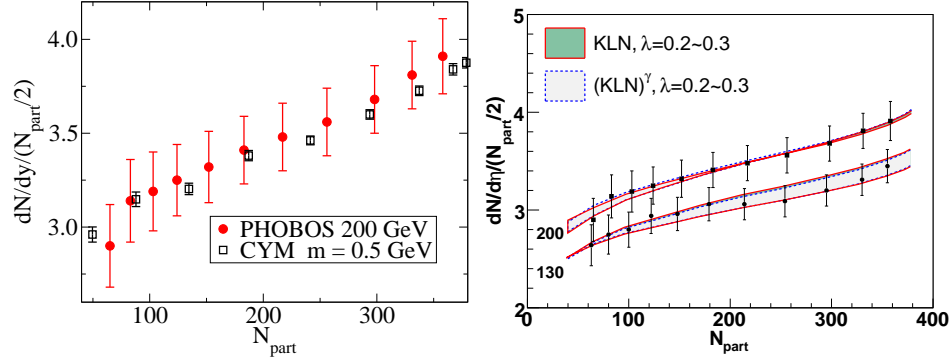


Fig. 10. Centrality dependence of the multiplicity. Left: CYM calculation⁸⁴. Right: KLN calculation⁸⁵.

sions are independent of each other. Using a simple ansatz for the dependence of the charged particle multiplicity on N_{part} and N_{coll} one can then divide the events of the whole minimum bias data set into centrality classes and estimate the typical impact parameters corresponding to each class (see⁸³ for a review of Monte Carlo Glauber modeling).

Besides the ZDC data there are few ways to independently check the consistency of the MC Glauber framework for understanding the collision geometry. One is nevertheless comforted by a general impression that the picture seems to work very consistently, depending weakly on the details of the MC Glauber model and successfully parametrizing a wide range of phenomena. In particular it turns out that the bulk particle production mechanism is such that the charged particle multiplicity is roughly proportional to the number of participant (“wounded”) nucleons, with a constant of proportionality increasing slightly as one goes to more central collisions. A MC Glauber computation is, however, merely a parametrization of data: it does not contain any dynamics and therefore does not provide a microscopical explanation of the particle production mechanism.

5.1. Centrality dependence of multiplicity

The approximate proportionality of $dN/d\eta$ to N_{part} is a natural result in the CGC framework. The saturation scale Q_s being the only dimensionful parameter in the problem the multiplicity per unit area should be $\sim 1/Q_s^2$. In a fully central collision the saturation scales of the two nuclei at a transverse coordinate \mathbf{x}_T are equal to each other and proportional to the nuclear thickness (and therefore to N_{part}) at the point \mathbf{x}_T ; integrating over the transverse plane gives a multiplicity proportional to N_{part} .

For noncentral collisions the situation at a fixed transverse coordinate \mathbf{x}_T is asymmetric since the two saturation scales Q_s^A and Q_s^B are not equal to each other. In this case the multiplicity can also have a dependence on Q_s^A/Q_s^B . Parametrically,

the spectrum of produced gluons in this case behaves^{48,57} as

$$\frac{dN}{d^2\mathbf{x}_T d^2\mathbf{p}_T} \sim \ln(p_T), \quad p_T < Q_{s1} \quad (31)$$

$$\sim \frac{Q_{s1}^2}{p_T^2}, \quad Q_{s1} < p_T < Q_{s2} \quad (32)$$

$$\sim \frac{Q_{s1}^2 Q_{s2}^2}{p_T^4}, \quad p_T > Q_{s2}, \quad (33)$$

where Q_{s1} and Q_{s2} are the smaller and larger of the saturation scales Q_s^A and Q_s^B . Integrated over transverse momenta, this gives

$$\frac{dN}{d^2\mathbf{x}_T} \sim Q_{s1}^2 \quad (34)$$

neglecting logarithmic corrections $\sim \ln(Q_{s2}/Q_{s1})$.

Both the CYM and KLN types of calculations^{28,84,86} reproduce quite well the experimental data on the centrality dependence of the multiplicity, as shown in Fig. 10. In the CYM calculation all the deviations from a strict proportionality $dN/d\eta \sim N_{\text{part}}$ come from the (parametrically logarithmic) deviations from the strict proportionality to the smaller one of the saturation scales, Eq. (34). In the KLN calculations, especially in the earlier versions where the geometry was treated in a more simplified way, a significant part of the deviation from $dN/d\eta \sim N_{\text{part}}$ was argued to result from the running of the coupling constant in $dN/d\eta \sim \pi R_A^2 Q_s^2 / \alpha_s(Q_s)$. The deviations from a number of participant scaling in the experimental data are small enough that they do not allow one to discriminate between the relative importance of these effects.

5.2. Eccentricity of the initial state

A striking signal of collective behavior of the matter produced at RHIC is elliptic flow (for a recent review, see⁸⁷). Comparing hydrodynamical calculations with flow is a way to address fundamental properties of the medium, such as the viscosity, but this comparison requires understanding of the initial conditions of the hydrodynamical evolution, particularly the initial eccentricity for elliptic flow. The original general consensus some years ago was that ideal hydrodynamics is in good agreement with the experimental data. Among other caveats this general conclusion also supposes that one is relatively free to choose the initial conditions—in particular the transverse geometry—of the hydrodynamical calculation to fit the experimental data (see e.g. the thorough comparison of initial conditions⁸⁸). This claim has had to be reevaluated more recently after it was argued (using a KLN-type calculation^{89,90,91}) that CGC results in a larger initial eccentricity than traditionally used in hydrodynamical calculation (mostly participant or wounded nucleon, often called “Glauber” initial conditions). This leaves more room for viscosity in the hydrodynamical evolution. The CGC estimate has now settled to a lower value than

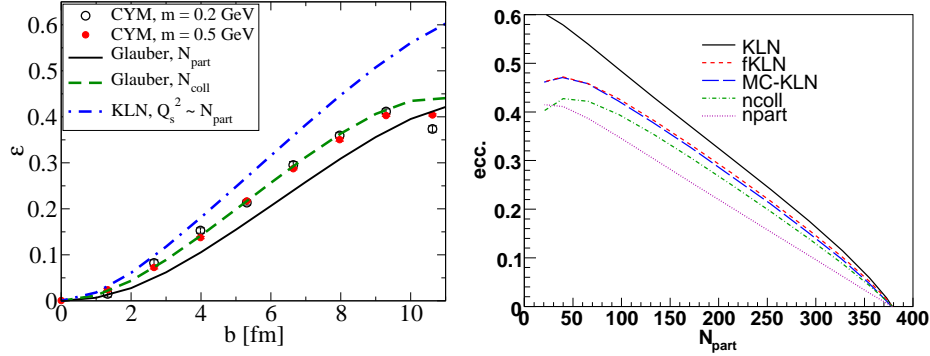


Fig. 11. Left: The original KLN eccentricity⁸⁹ compared to the CYM result⁸⁴. Right: A subsequent revision of the KLN model was to reformulate the nonuniversal saturation scale in terms of fluctuations in the participant nucleons led to a lower eccentricity estimate (“fKLN”)⁸⁵ practically in agreement with the CYM result and very close to binary collisions scaling.

first argued in⁸⁹ due to further developments that we will outline below. The result remains, however, that generically CGC calculations tend to predict an initial state with an eccentricity close to or slightly above N_{coll} scaling, which is larger than often used in hydrodynamics. The eccentricity obtained in the CYM calculation is demonstrated in Fig. :11. Everything else staying equal, the larger eccentricity of the initial state can be compensated by the effect of a larger viscosity in order to produce the observed elliptic flow v_2 . When other parameters in the fit are also allowed to change, the situation can become more complicated and, in some cases, contrary to this basic intuition. For example in the “Knudsen number” fit of⁹² assuming a finite cross section (and thus deviations from ideal hydrodynamics including viscosity) also the equation of state was allowed to vary as a fit parameter. The result of the fit was that the CGC initial conditions actually corresponded to a smaller viscosity (larger cross section); the observed smaller v_2 being achieved by a softer equation of state ($c_s = 0.22$ vs 0.3 for the Glauber initial conditions).

As we saw previously, in the case of two different saturation scales at a point in the transverse plane, the gluon multiplicity only depends on the smaller one of the two. The initial eccentricity, on the other hand, is computed from the energy density^f, which behaves parametrically as $Q_{s1}^2 Q_{s2}$, where again $Q_{s1} < Q_{s2}$. In the original KLN calculations the transverse coordinate dependence of the saturation scale was taken as $Q_s^A(\mathbf{x}_T) \sim n_{part,A}(\mathbf{x}_T)$, where $n_{part,A}(\mathbf{x}_T)$ is the density of participating nucleons in nucleus A. This has the advantage of being directly connected to the well established Glauber modeling of the geometry also used to bin

^f In particular in the CYM calculation, where one is explicitly faced with the fact that the energy density is practically the only local gauge invariant observable available. The gluon spectrum is determined by Fourier-transforming the field modes and is therefore necessarily nonlocal at a scale $1/p_T$. In a (semi)analytical calculation such as KLN one can formally evade this problem.

the experimental data. To understand the effect of this prescription on the calculated eccentricity one must study what happens in a noncentral collision. The important region for this is the one at the edge of one of the nuclei (nucleus A) and the center of the other one (B). In this case the definition leads to both saturation scales being small (since $n_{\text{part,B}}$ goes to zero outside of nucleus A). This is conceptually problematic, since one would expect the saturation scale to be large in the center of nucleus B. The KLN prescription is therefore nonuniversal: the value of Q_s^B is not a property of nucleus B alone, but is determined by a final state effect; namely the presence or not of the other nucleus A at a given transverse coordinate. Since $\varepsilon \sim Q_s^B Q_s^{A^2}$ in this region, this prescription leads to a suppression in the energy density in the edge of the interaction region and a larger eccentricity, basically independently of the precise form of the unintegrated gluons distribution (see Fig. 12). To remedy this nonuniversality problem in the KLN model it has subsequently been reformulated into what is known as the fKLN⁸⁵ (fluctuating KLN) model, where one first introduces explicitly the nucleon-nucleon cross section to determine whether a given nucleon participates in the scattering. After this step the resulting gluon spectrum is the calculated with universal saturation scales in the two nuclei. The fKLN model, has practically by construction, the property that a) the saturation scales are universal, b) the original KLN centrality dependence of the multiplicity is reproduced (due to the property (34)) and c) it reproduces event-by-event fluctuations⁸⁶ that are close to ones given by Monte Carlo Glauber calculations. (For experimental results on v_2 fluctuations see e.g. Ref.⁹³). The resulting eccentricity, as shown in Fig. 11 (right) becomes smaller, closer to the result (similar to N_{coll} scaling) obtained in the straightforward and universal CYM calculation. The price to pay for this modification is a nonuniversality of another kind: namely the k_T -factorized formalism becomes different for AA-collisions than it is for the case of proton-proton collisions. In the treatment of AA collisions in the fKLN formulation there is an additional step of computing first a collision probability of individual constituents of the colliding objects (nucleons in a nucleus) which is not invoked in the pp-case. In other words, nuclei are, even at high energy and high p_T , not treated as consisting of quarks and gluons, but as fundamentally more complicated objects to which the usual (collinear) QCD factorization theorems do not apply. One curious consequence of this feature is that the saturation scale of the nucleus in the fKLN model approaches a constant, not zero, at arbitrarily large distances outside the nucleus.

6. Correlations in the glasma

So far we have discussed how the CGC picture of the small x nuclear wavefunction can be used to compute bulk properties of the initial state of a heavy ion collision. Experiments do not probe this initial state directly, because the system goes through a complicated time evolution before the hadronization stage. A good candidate for a more direct experimental probe of the glasma stage is provided by

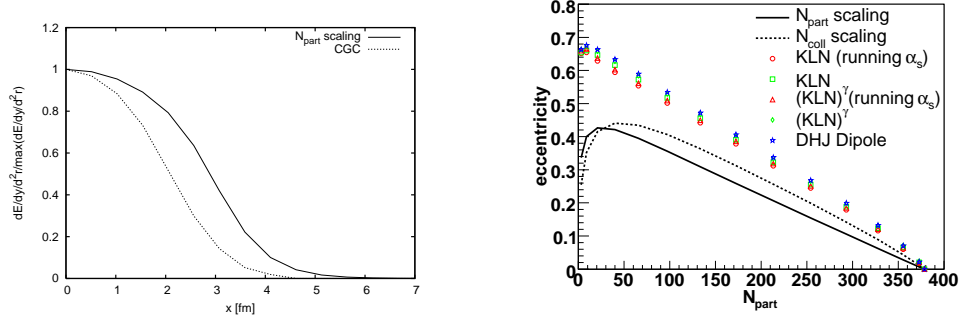


Fig. 12. Left: energy density as a function of the transverse coordinate in the original KLN definition compared to participant number scaling. Right: the KLN eccentricity for different unintegrated gluon distribution parametrizations. Plots from Ref.⁹⁰.

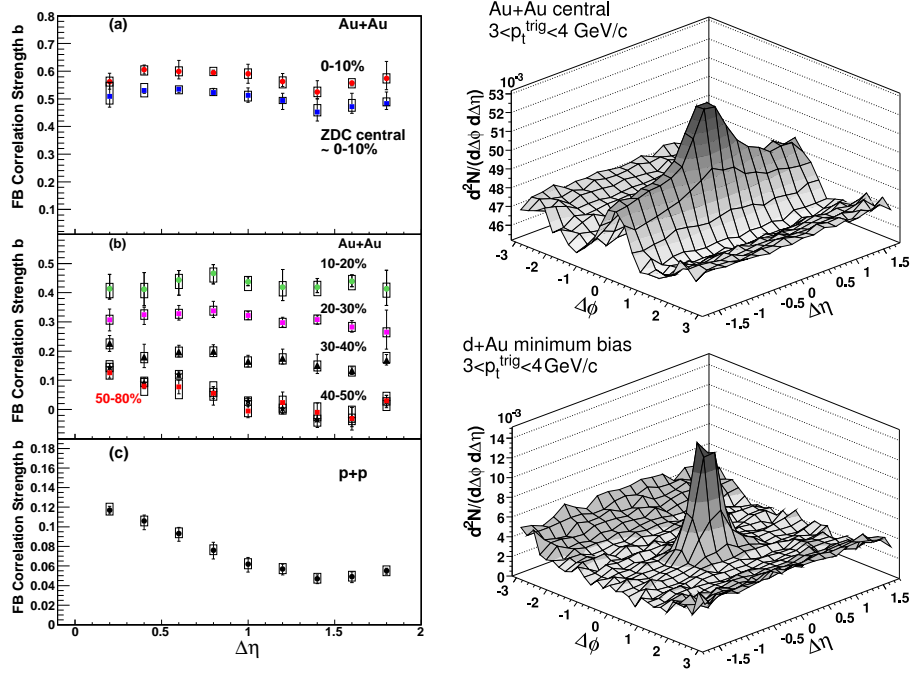


Fig. 13. Left: forward-backward multiplicity correlations from STAR⁹⁴ Right: Experimental 2-particle correlation data⁹⁵ in AuAu and dAu collisions, showing the elongated ridge structure in the former case.

different kinds of correlation measurements, and they have recently been a focus of both experimental and theoretical activity. Particles that are produced far in rapidity can, by causality, only be correlated at early times, and should therefore

be directly related to the properties of the glasma^g. Examples of these long range correlations are the “Ridge” structure of two particle correlations in central heavy ion collisions^{96,97,95} and of long range rapidity correlations in particle multiplicities^{94,98} (see Fig. 13)^h. Another interesting correlation measurement are electric charge-reaction plane correlations^{100,101} that can be due to CP-violating fluctuations in the initial stage. As we shall argue, these correlations also arise naturally in the glasma. Correlations between the electric charge and the reaction plane are most likely mediated by the magnetic field caused by the noncentral collision of two positively charged ions; it is hard to think of another quantity that would as directly couple to both the reaction plane direction and the electric charge. Since this magnetic field dies away very fast with τ , the QCD part of the explanation must be sensitive to the gluon fields at the earliest stage of the collision. In the following we shall discuss some features of how these correlations can be understood in the glasma framework.

6.1. Multigluon correlations in the boost invariant case

In Sec. 2.3 we argued that the leading logarithmic corrections to particle production should be factorizable into the distributions describing the sources. As the argument is essentially one of causality, it applies also to multigluon production (a more formal proof is given in Ref.²⁷). The case is particularly straightforward when the rapidity differences between the produced gluons are small enough compared to $1/\alpha_s$, so that at leading order one does not need to resum the radiation of additional gluons between the measured ones. In this case the rapidity structure is indeed a trivial one: when observing gluon fields within a rapidity window smaller than $1/\alpha_s$; all the gluons are sensitive to the same configuration of sources and the gluon fields are boost invariant.

In fact, gluon correlations in AA-collisionsⁱ are in a sense simpler than in more dilute systems. To understand why let us first formally evaluate the leading contribution in a dense-dense collision. Consider the probability distribution of the number of gluons produced in a small rapidity interval. It is convenient to define a generating functional

$$\mathcal{F}[z(\mathbf{p})] = \sum_{n=0}^{\infty} \frac{1}{n!} \int \left[\prod_{i=1}^n d^3\mathbf{p}_i (z(\mathbf{p}_i) - 1) \right] \frac{d^n N_n}{d^3\mathbf{p}_1 \cdots d^3\mathbf{p}_n}. \quad (35)$$

The Taylor coefficients of \mathcal{F} around $z = 1$ correspond to the moments of the probability distribution; integrated over the momenta of the produced gluons they

^gAlthough when making precise estimates one must be more careful and distinguish spacetime, momentum space and pseudorapidity and understand shorter range correlations such as those from hadronization.

^hThe interpretation of this multiplicity correlation data is somewhat puzzling because of the interplay with the impact parameter induced, purely geometrical, correlations⁹⁹.

ⁱBy “AA” what is meant here is really the formal power counting situation when the color sources of both nuclei are strong, as we shall discuss shortly.

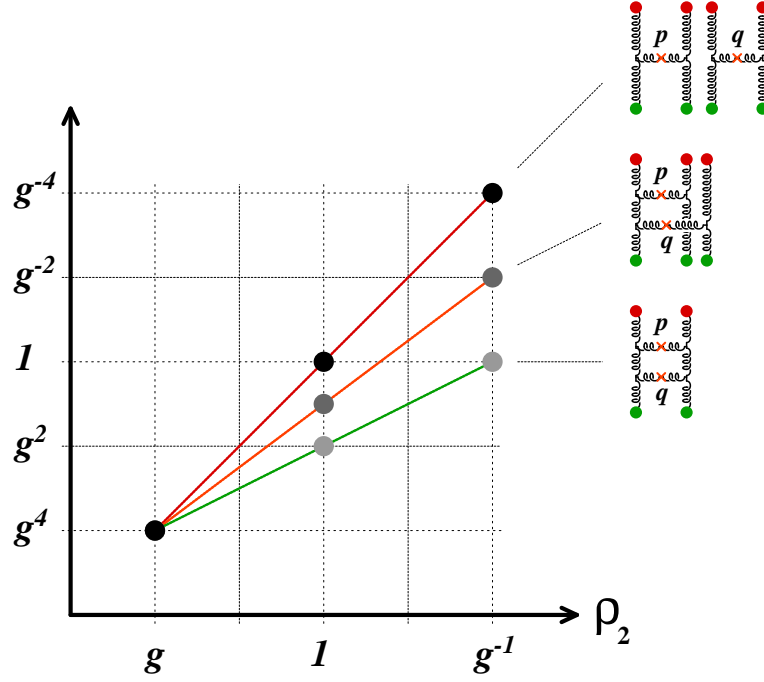


Fig. 14. Relative importance of connected and disconnected diagrams to the two gluon correlation function. One of the color charge densities is considered large, $\rho_1 \sim 1/g$, whereas the other is allowed to vary between the “AA” case $\rho_2 \sim 1/g$ and the “pA” one $\rho_2 \sim g$. The order of the disconnected diagram, on top, is $g^4 \rho_1^4 \rho_2^4$, whereas the interference diagram in the middle is $g^4 \rho_1^3 \rho_2^3$ and the connected one, lowest, is $g^4 \rho_1^2 \rho_2^2$. In the “AA” case the disconnected diagram dominates, for the “pA” case all three are equally important. In the dilute “pp” limit only the connected diagram matters and both gluons are produced from the same BFKL ladder.

are

$$\langle N \rangle \quad \langle N(N-1) \rangle \quad \dots \quad \langle N(N-1) \dots (N-n+1) \rangle. \quad (36)$$

The result of Ref. 27 is that when these moments are calculated to NLO accuracy, the leading logarithms can be resummed into the JIMWLK evolution of the sources; completely analogously to the single inclusive gluon distribution. The resulting probability distribution can be written as:

$$\frac{d^n P_n}{d^3 \mathbf{p}_1 \dots d^3 \mathbf{p}_n} = \int_{\rho_1, \rho_2} W_Y[\rho_1] W_Y[\rho_2] \frac{1}{n!} \frac{dN}{d^3 \mathbf{p}_1} \dots \frac{dN}{d^3 \mathbf{p}_n} e^{-\int d^3 \mathbf{p} \frac{dN}{d^3 \mathbf{p}}}. \quad (37)$$

Here the factors $\frac{dN}{d^3 \mathbf{p}_n}$ denote the multiplicities corresponding to the leading order classical fields.

The probability distribution (37) has been derived to the leading order in a weak coupling expansion in α_s , and resumming leading logarithms of $1/x$. In this power counting, each insertion of the external color source contributes a factor $\rho \sim 1/g$, so

that the saturation scale $g^2\langle\rho\rho\rangle\sim Q_s^2$ is taken to have no powers of the coupling. This leads to the glasma fields being parametrically $A_\mu\sim 1/g$ and $\frac{dN}{d^3\mathbf{p}_n}\sim 1/\alpha_s$ at the dominant classical level. An additional insertion of a color source then does not change the power of α_s of the result, since the $1/g$ in ρ compensates the additional g in the three gluon vertex that attaches it into the diagram. Thus the leading contribution is given by a sum of all tree diagrams with an arbitrary number of insertions of the classical source¹⁰²; a computation that has to be done numerically. In the language of BFKL physics, the dominant contribution to n -gluon production in this “AA” case comes from cutting one rung in n distinct BFKL ladders. Producing two gluons from the same ladder is suppressed by the weak coupling compared to this “disconnected” contribution. In the “pA” or “pp” power counting, on the other hand, one or both of the sources ρ are assumed to be weak. For example at large x the color source consists of a number $\mathcal{O}(1)$ of charged (valence-like) partons, each with a charge $\sim g$ (times a color factor). This leads to $\rho\sim g$, and additional insertions of such a weak external color charge lead to a contribution that is suppressed at weak coupling. Thus in the “pp” case the dominant contribution to multigluon production is achieved by producing all the gluons from the same ladder, minimizing the number of insertions of the color source. Whereas in the AA-case the dominant contribution comes from (complicated) tree diagrams and has a classical field interpretation, in the “pp” case the n gluons are produced from the same ladder, which is an $n-1$ -loop diagram. In the “pA” case, when $\rho_A\sim 1/g$ and $\rho_p\sim g$ both the connected (loop) and disconnected digrams are parametrically equally important. This structure is illustrated in Fig. 14, where the contributions of the “disconnected” and “connected” diagrams and their interference term are evaluated for the case of $\rho_1\sim 1/g$ and ρ_2 having different parametric dependences on g . In practice, however, many applications to two particle correlations in the “pA” case only the connected part has been considered (see e.g. ¹⁰³ for a discussion).

Note that the Poissonian-looking form of the result is to some extent an artifact of our choosing to develop and truncate precisely the moments Eq. (35) that are simply $\langle N \rangle^n$ for a Poissonian distribution. Since in our power counting $N\sim 1/\alpha_s$, any contributions that would make the distribution Eq. (37) deviate from the functional form are of higher order in the weak coupling expansion of the moments (35) and are neglected in the calculation unless they are enhanced by large logarithms of x . It should also be emphasized that in spite of appearances of Eq. (37) the probability distribution is in fact not Poissonian. To understand the nontrivial nature of this result it must be remembered that the individual factors of $\frac{dN}{d^3\mathbf{p}_i}$ in Eq. (37) are all functionals of the *same* color charge densities $\rho_{1,2}$; thus the averaging over the ρ 's induces a correlation between them. These correlations are precisely the leading logarithmic modifications to the probability distribution; they have been resummed into the distributions W_y ; the functional form of the multigluon correlation function *under* the functional integral in Eq. (37) is the same as at leading order. The fact that the dominant contribution is disconnected for fixed sources

32 *T. Lappi*

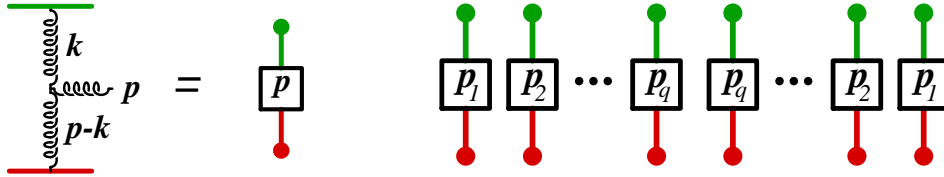


Fig. 15. Left: Building block, Lipatov vertex coupled to two sources. Right: combinatorics of the sources. The combinatorial problem is to connect the dots on the upper and lower side (left- and right moving sources) pairwise.

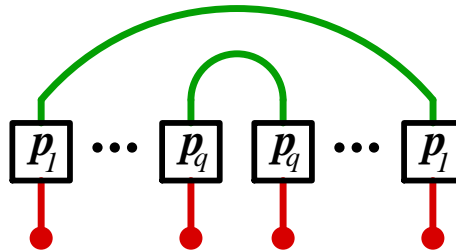


Fig. 16. Dominant contributions are “rainbow” diagrams, where on one side (left- or rightmoving sources) the same sources in the amplitude and the complex conjugate are connected to each other.

and becomes correlated only when one averages over the distribution of ρ has the physical interpretation that the dominant correlations in the systems are the ones enhanced by large logarithms of x and are *already present in the wavefunction* before the collision. Because of this the calculation of multigluon correlations is in fact simplified in the strong field limit ^{60,104}.

6.2. *The ridge and the negative binomial*

We can then apply this formalism to the calculation of the probability distribution of the number of gluons in the glasma ^{105,106,107}. We shall assume the “AA” power counting of sources that are parametrically strong in g , but nevertheless work to the lowest nontrivial order in the color sources. Formally this would correspond to a power counting $\rho \sim g^{\epsilon-1}$ with a small $\epsilon > 0$. In this limit, as we have discussed, the dominant contributions to multiparticle correlations come from diagrams that are disconnected for fixed sources and become connected only after averaging over the color charge configurations.

Working with the MV model Gaussian probability distribution

$$W[\rho] = \exp \left[- \int d^2 \mathbf{x}_T \frac{\rho^a(\mathbf{x}_T) \rho^a(\mathbf{x}_T)}{g^4 \mu^2} \right] \quad (38)$$

computing the correlations in the linearized approximation is a simple combinato-

rial problem. Each gluon is produced from two Lipatov vertices (see Fig. 15 left), one in the amplitude and the other in the complex conjugate. The combinatorial factor is obtained by counting the different ways of contracting the sources pairwise (see Fig. 15 right). The dominant contributions are “rainbow” diagrams, Fig. 16, where on the side of one of the sources a line with momentum \mathbf{p}_T in the amplitude is connected to a line with the same momentum in the complex conjugate amplitude. These contributions dominate because they contain a maximally infrared divergent integral in the momentum circulating in the lower (“non-rainbow”) side of the diagram. This divergence is then regulated by the transverse correlation scale of the problem, Q_s . When integrated over the momenta of the produced gluons one obtains the factorial moments of the multiplicity, which define the whole probability distribution. The result of the combinatorial exercise is that the number of contributing diagrams, each with an equal contribution, is $2^q(q-1)!$. The probability distribution can be expressed in terms of two parameters, the mean multiplicity \bar{n} , and a parameter k describing the width of the distribution. The factorial moments $m_q \equiv \langle N^q \rangle - \text{disc.}$ are

$$m_q = (q-1)! k \left(\frac{\bar{n}}{k} \right)^q \quad (39)$$

with parameters k and \bar{n} given by

$$k \approx \frac{(N_c^2 - 1) Q_s^2 S_\perp}{2\pi} \quad (40)$$

$$\bar{n} = f_N \frac{1}{\alpha_s} Q_s^2 S_\perp. \quad (41)$$

These moments define a *negative binomial* distribution, which has been used as a phenomenological observation in high energy hadron and nuclear collisions already for a long time¹⁰⁸. In terms of the glasma flux tube picture this result has a natural interpretation. The transverse area of a typical flux tube is $1/Q_s^2$, and thus there are $Q_s^2 S_\perp = N_{\text{FT}}$ independent ones. Each of these radiates particles independently into $N_c^2 - 1$ color states in a Bose-Einstein distribution (see e.g.¹⁰⁹). A sum of $k \approx N_{\text{FT}}(N_c^2 - 1)$ independent Bose-Einstein-distributions is precisely what defines a negative binomial distribution.

An important special case of this result (and one that was first obtained independently from the general derivation of the multiplicity distribution in¹⁰⁵) are two gluon correlations. Similarly as in Sec. 4 one can argue that they should be closely related to the two particle correlations observed in the final state. There are two major ingredients in the “glasma flux tube¹⁰⁵” explanation for the ridge:

- The long range longitudinal structure is provided by the approximately boost invariant glasma fields. The fields are correlated at a (transverse) length scale $1/Q_s$ which enables one to estimate the strength of the correlation.
- The narrow azimuthal structure is explained by a collimating effect¹¹¹ from the strong radial flow generated in the hydrodynamical stage.

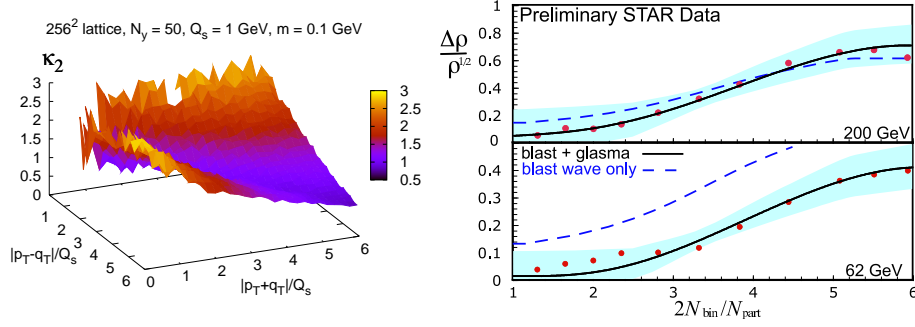


Fig. 17. Left: Two-gluon correlation in a numerical CYM evaluation in the MV model⁷⁴. Right: Strength of the ridge correlation from a calculation including the initial correlations from the glasma fields and a blast-wave parametrization of hydrodynamical evolution¹¹⁰.

It has become conventional to parametrize the two particle correlation function in terms of the single particle spectra and a geometrical factor related to the number of flux tubes as

$$\frac{C_2(\mathbf{p}, \mathbf{q})}{\left\langle \frac{dN}{dy_p d^2\mathbf{p}_T} \right\rangle \left\langle \frac{dN}{dy_q d^2\mathbf{q}_T} \right\rangle} = \kappa_2(\mathbf{p}_T, \mathbf{q}_T) \frac{1}{S_\perp Q_s^2}, \quad (42)$$

wherer C_2 is the two-particle correlation function

$$C_2(\mathbf{p}, \mathbf{q}) \equiv \left\langle \frac{d^2 N_2}{dy_p d^2\mathbf{p}_T dy_q d^2\mathbf{q}_T} \right\rangle - \left\langle \frac{dN}{dy_p d^2\mathbf{p}_T} \right\rangle \left\langle \frac{dN}{dy_q d^2\mathbf{q}_T} \right\rangle. \quad (43)$$

Generally κ_2 is expected to be a number of order one. It is a constant $\kappa_2 \approx 0.4^j$ (up to logarithms) in the dilute limit calculation^{105,107}, but there is no reason for it to be a constant in a full calculation. The scaled correlation function has recently been evaluated⁷⁴ in the MV model, with the result typically being very close to $\kappa_2 \approx 1$, but with some dependence on \mathbf{p}_T and \mathbf{q}_T . The result of this numerical calculation is shown in Fig. 17 as a function of $|\mathbf{p}_T - \mathbf{q}_T|$ and $|\mathbf{p}_T + \mathbf{q}_T|$. The experimentally observed quantity is denoted as $\Delta\rho/\sqrt{\rho_{\text{ref}}}(\Delta\varphi)$. Assuming a blast-wave parametrization of the hydrodynamical evolution the value at $\Delta\varphi = 0$ can be related to κ_2 as¹⁰⁵

$$\begin{aligned} \frac{\Delta\rho}{\sqrt{\rho_{\text{ref}}}}(\Delta\varphi = 0) &= \frac{dN}{dy} \cdot \frac{C_2(\mathbf{p}, \mathbf{q})}{\left\langle \frac{dN}{dy_p d^2\mathbf{p}_T} \right\rangle \left\langle \frac{dN}{dy_q d^2\mathbf{q}_T} \right\rangle} \left(\gamma_B - \frac{1}{\gamma_B} \right) \\ &= \frac{K_N}{\alpha_s} \left(\gamma_B - \frac{1}{\gamma_B} \right), \end{aligned} \quad (44)$$

where $K_N = \kappa_2/13.5$ for an SU(3) gauge theory (based on the relation between the multiplicity and $Q_s^2 S_\perp$ discussed in Sec. 4.) Here γ_B is the average radial boost in

^jAfter correcting for incorrect constant factors in the original calculation of¹⁰⁵; see⁷⁴ for a discussion.

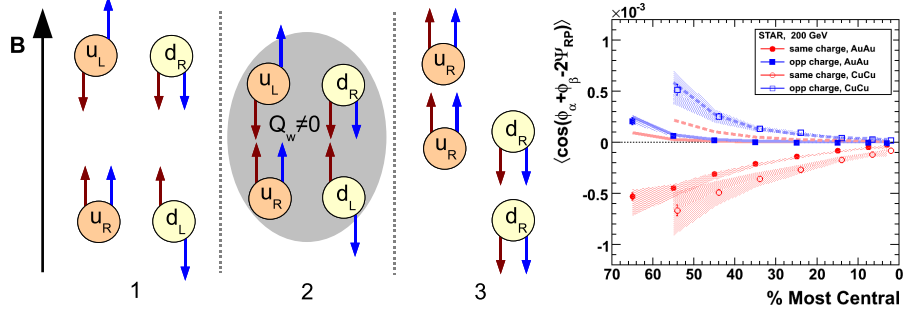


Fig. 18. Left: Illustration of the chiral magnetic effect. In situation 1 the spins (blue or right arrow) of the positively charged u quarks are aligned with the external magnetic field \vec{B} , and those of the d quarks against it. The momenta (red or left arrow) of the right handed quarks are in the direction of the spin and those of the left-handed quarks are opposite to it. After an external color field configuration with nonzero Chern-Simons number an excess of right-handed quarks is present. This leads to an excess of momentum in the direction of \vec{B} for the u quarks and against \vec{B} for the d 's, i.e. an electric dipole moment. Right: Correlation data showing a signal for a like side correlation for same charge pairs from¹⁰¹. The solid (AuAu) and dashed (CuCu) lines represent the estimates of the effect of 3-particle correlations based on HIJING.

the framework of a blast wave model. From the RHIC data⁹⁶, one can estimate that $\Delta\rho/\sqrt{\rho_{\text{ref}}}(\Delta\varphi = 0) = 1/\sqrt{2\pi\sigma_\varphi^2}$, with $\sigma_\varphi = 0.64$. Combining this with Eq. (44), one obtains

$$\kappa_2^{\text{BW}} \sim \frac{0.7}{(\gamma_B - \frac{1}{\gamma_B})}, \quad (45)$$

for $\alpha_s = 0.5$ and where the superscript denotes that this is a crude estimate extracted from experiment using a blast-wave parametrization. For an average blast wave radial velocity $V_r = 0.6$, this gives $\kappa_2^{\text{BW}} \sim 1.5$; for $V_r = 0.7$, one obtains $\kappa_2^{\text{BW}} \sim 1$. A comparison of this parametrization to experimental data is shown in Fig. 17. For more detailed phenomenological studies we refer the reader to^{110,112}. In spite of the increasingly detailed modeling of the final stage effects there remains some uncertainty in the strength of the correlation. More detailed understanding of the strength of the initial correlations from JIMWLK evolution and further comparisons of realistic hydrodynamical calculations are still needed to clarify these issues.

6.3. Chiral magnetic effect

There have been several discussions¹¹³ of the possibility of observing event-by-event CP-violating fluctuations in heavy ion collisions. The discussion originally focused on the possibility of generating these fluctuations in the thermal phase of the collision process. However, the large longitudinal classical color fields in the glasma provide a very natural framework for the phenomenon to occur^{114,11}.

Parity violation in a large classical field configurations can occur when one has a large Chern-Simons charge N_{CS} , which is the time component of the topological current K^μ ; $\partial_\mu K^\mu = \tilde{F}_a^{\mu\nu} F_{\mu\nu}^a$, where $\tilde{F}^{\mu\nu} = \frac{1}{2}\epsilon^{\mu\nu\rho\sigma} F_{\rho\sigma}$. In terms of the gauge potentials this Chern-Simons current is

$$K^\mu = \epsilon^{\mu\nu\rho\sigma} A_\nu^a \left(F_{\rho\sigma}^a + \frac{g}{3} f^{abc} A_\rho^b A_\sigma^c \right). \quad (46)$$

In the strict boost invariant case N_{CS} is suppressed by topological reasons, which has been seen in numerical simulations¹¹⁴. But in the presence of fluctuations that break boost invariance the natural (unsuppressed by the weak coupling) strength of N_{CS} is expected to be seen, although this has not yet been confirmed by an explicit calculation. When quarks are produced in the color field, a nonzero value of the Chern-Simons charge leads to an excess of quarks of a given chirality being produced. Due to symmetry the average of N_{CS} over a large number of events will be zero, but the fluctuations will be large and measurable. The magnitude of the fluctuations can again be estimated using the fact that the systems consists of correlated areas of size $1/Q_s^2$ in the transverse plane. The number of these domains, each having charge ~ 1 , is $\sim \pi R_A^2 Q_s^2$. The sum of these independent charges will fluctuate around zero with magnitude $\sqrt{\langle N_{\text{CS}}^2 \rangle} \sim \sqrt{N} \sim Q_s R_A$.

The experimental manifestation of parity violation in heavy ion collisions happens through the ‘‘chiral magnetic effect’’¹¹⁵ (see Fig. 18). In a noncentral collision there is an external magnetic field perpendicular to the reaction plane caused by the positive charges of the ions. The spins of the quarks become correlated with this magnetic field. In the presence of a net chirality this causes the momenta of the quarks to be correlated with their electric charge times the magnetic field. This means that one is generating, event by event, a net electric dipole moment (a vector) that is correlated with the reaction plane (pseudovector), a classical signal of CP violation analogous to the elusive neutron electric dipole moment. Such a correlation between the electrical charges and momenta of the produced particles with the reaction plane has now, after being predicted by the theory, been observed by the STAR experiment^{100,101} (see however¹¹⁶ for a discussion of other effects leading to similar experimental signatures).

6.4. Rapidity dependence of two gluon correlation

The same power counting argument that qualitatively distinguishes AA collisions from ones involving a dilute probe also applies to correlations between gluons at larger rapidity separations. When producing two gluons from the same BFKL ladder (which is the dominant mechanism in pp and pA) momentum conservation causes the dominant long range (in rapidity) correlation to be back-to-back in azimuthal angle. A long range correlation on the near side that leads to the ridge comes from diagrams that are disconnected for fixed sources and only become connected at the level of the source distribution. To calculate the rapidity dependence of the ridge one must therefore go beyond the leading order boost invariant clas-

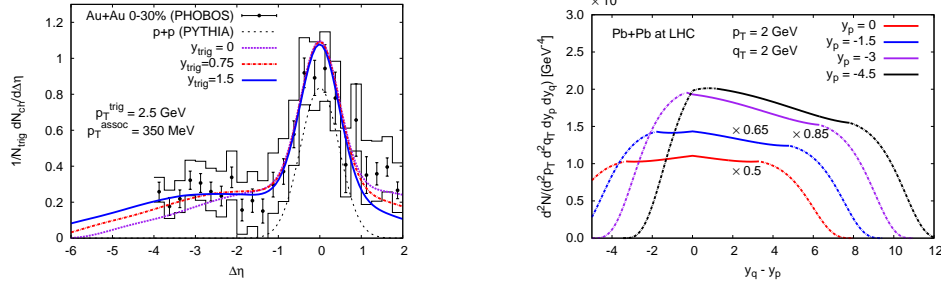


Fig. 19. Left: Comparison of a two-particle correlation computed using Eq. (53) supplemented with a short-range correlation contribution from PYTHIA with PHOBOS data. Right: comparison Left: Rapidity correlation at LHC energies k_T -factorization approximation. Plots from¹¹⁷.

sical fields. The first step in this direction is to compute the leading logarithmic corrections, more precisely to resum corrections that are proportional to $\alpha_s(y_p - y_q)$, where y_p and y_q are the rapidities of the two produced gluons. In the dense-dense case when the correlations are dominated by those present in the color sources, this is achieved by including the JIMWLK evolution between the rapidities of the produced gluons^{118,119}.

The crucial aspect of JIMWLK evolution for unequal rapidity correlations is to realize that the probability distribution $W[\rho]$ should really be understood as a distribution for *trajectories* of the color charge densities (or in practice the Wilson lines derived from them) along path to larger rapidities. In this sense the formalism contains more physical information than just the equation for $W_y[U(\mathbf{x}_T)]$; the probability distribution at a single rapidity y . Namely, it also gives the combined probability distribution for Wilson lines at different rapidities

$$W_{y_1 \dots y_n}[U_1(\mathbf{x}_T), \dots, U_n(\mathbf{x}_T)], \quad (47)$$

or in a formulation in that is continuous in rapidity $W[U(\mathbf{x}_T, y)]$. We can formally return from the distribution of trajectories to a distribution of Wilson lines at one individual rapidity as

$$W_y[U(\mathbf{x}_T)] \equiv \int [DU(y, \mathbf{x}_T)] W[U(y, \mathbf{x}_T)] \delta[U(\mathbf{x}_T) - U(y, \mathbf{x}_T)]. \quad (48)$$

Knowing the general (multiple rapidity) probability distribution will enable us to compute the correlations between Wilson lines, and consequently of physical observables such as the multiplicities, at different rapidities. A transparent interpretation of this can be obtained in the Langevin formulation of high energy evolution¹²⁰, where one explicitly constructs the ensemble of Wilson lines from solutions of a nonlinear Langevin equation. The Langevin formulation is also the one used in the (numerical) full solution of the JIMWLK equation^{121,122}.

Knowing that the correlation follows from a Langevin equation imposes an ad-

ditional structure (of a Markovian process) on the joint probability distribution:

$$W_{y_p, y_q} [U^p, U^q] = G_{y_p - y_q} [U^p, U^q] W_{y_q} [U^q], \quad (49)$$

where the JIMWLK Green's function G is determined by the initial condition

$$\lim_{y_p \rightarrow y_q} G_{y_p - y_q} [U^p, U^q] = \delta (U^p(\mathbf{x}_T) - U^q(\mathbf{x}_T)) \quad (50)$$

and the requirement that it must satisfy the JIMWLK equation

$$\partial_{y_p} G_{y_p - y_q} [U^p, U^q] = \mathcal{H} (U^p(\mathbf{x}_T)) G_{y_p - y_q} [U^p, U^q]. \quad (51)$$

This JIMWLK Green's function contains all the information, at the leading log level, of long range rapidity correlations in gluon production. This structure follows from the computation of the leading log part of 1-loop corrections to a wide class of observables that can be expressed in terms of correlators of the gluon fields at $\tau = 0$ (or equivalently in terms of the Wilson lines)

$$\langle \mathcal{O} \rangle_{\text{LLog}} = \int [DU_1(y, \mathbf{x}_T)] [DU_2(y, \mathbf{x}_T)] W [U_1(y, \mathbf{x}_T)] W [U_2(y, \mathbf{x}_T)] \mathcal{O}_{\text{LO}}. \quad (52)$$

A full (numerical) calculation of rapidity correlations in JIMWLK evolution is yet to be done. The first phenomenological applications of this framework¹¹⁷ follow the strategy of using the approximate linearized solution of the equations of motion used also in the boost invariant case reviewed in Sec. 6.2. One solves the two gluon correlation in terms of $\rho\rho$ -correlators^k, including unequal rapidity ones. Recognizing that due to the Markovian nature of the evolution $\langle \rho_y^A(\mathbf{x}_T) \rho_{y'}^A(\mathbf{y}_T) \rangle = \langle \rho_y^A(\mathbf{x}_T) \rho_y^A(\mathbf{y}_T) \rangle$, where y is the rapidity that is earlier in the evolution of nucleus A than y' , one can express the result in terms of equal-rapidity correlations of two ρ 's. To get a realistic estimate of the resulting rapidity dependence one then replaces the equal rapidity $\rho\rho$ correlators by solutions of the (running coupling) BK equation, denoted below as $\Phi(y, \mathbf{k}_T)$. The resulting k_T -factorized approximation is

$$C_2(\mathbf{p}, \mathbf{q}) = \frac{\alpha_s^2}{16\pi^{10}} \frac{N_c^2(N_c^2 - 1)S_\perp}{d_A^4 \mathbf{p}_T^2 \mathbf{q}_T^2} \int d^2\mathbf{k}_T \quad (53)$$

$$\left\{ \Phi_{A_1}^2(y_p, \mathbf{k}_T) \Phi_{A_2}(y_p, \mathbf{p}_T - \mathbf{k}_T) \left[\Phi_{A_2}(y_q, \mathbf{q}_T + \mathbf{k}_T) + \Phi_{A_2}(y_q, \mathbf{q}_T - \mathbf{k}_T) \right] \right.$$

$$\left. + \Phi_{A_2}^2(y_q, \mathbf{k}_T) \Phi_{A_1}(y_p, \mathbf{p}_T - \mathbf{k}_T) \left[\Phi_{A_1}(y_q, \mathbf{q}_T + \mathbf{k}_T) + \Phi_{A_1}(y_q, \mathbf{q}_T - \mathbf{k}_T) \right] \right\}.$$

Although the required symmetrizations make this formula look a bit awkward, the structure is in fact quite simple. The double inclusive gluon multiplicity is proportional to four unintegrated distributions (the single inclusive one being given by a convolution of two). This is a demonstration of our power counting argument; when the distributions are assumed to be large $\Phi \sim 1/\alpha_s$, this contribution to the correlation is $\sim 1/\alpha_s^2$. Producing the gluons from the same one BFKL ladder (“pp”

^k We are here assuming a Gaussian distribution so that no nontrivial higher cumulants contribute.

contribution) would be parametrically $\alpha_s^2 \Phi^2 \sim 1$. A result of the Markovian nature of the correlation is that the rapidity arguments are not symmetric; for example in the first term three out of the four distributions are evaluated at the rapidity y_p (earlier in the evolution of nucleus 1) and only one at the rapidity y_q . Implementing Eq. (53) leads to a very weak rapidity dependence and a normalization of the correlation in broad agreement with the experimental results, as seen in Fig. 19. One could assume that the decorrelation with rapidity could be faster in the full nonlinear JIMWLK evolution than the linearized version assumed in deriving the k_T -factorized approximation of the correlation. This would require combining the numerical JIMWLK evolution with a full CYM calculation of the multiplicity, which has not yet been performed.

7. Conclusions

We have emphasized in this short review the potential of the CGC framework as a description of the initial conditions of a heavy ion collision, based on weak coupling QCD. The CGC picture enables one to analyze DIS at small x , proton-nucleus collisions and the initial conditions in AA collisions in a single unified framework. As a weak-coupling first-principles QCD calculation there is a systematic way to compute higher order corrections to the results. We have seen that the basic features of bulk particle production in AA collisions, such as the collision energy, rapidity and centrality dependence can be well understood in terms of a single dominant momentum scale Q_s present in the high energy nuclear wavefunction. An area of recent and ongoing activity are multiparticle correlations, which have a high potential of giving direct experimental access to initial state of the collision.

Acknowledgements

The author is supported by the Academy of Finland, project 126604.

References

1. **BRAHMS** collaboration, I. Arsene *et. al.*, *Nucl. Phys.* **A757** (2005) 1 [arXiv:nucl-ex/0410020]; **PHENIX** collaboration, K. Adcox *et. al.*, *Nucl. Phys.* **A757** (2005) 184 [arXiv:nucl-ex/0410003]; **PHOBOS** collaboration, B. Back *et. al.*, *Nucl. Phys.* **A757** (2005) 28 [arXiv:nucl-ex/0410022]; **STAR** collaboration, J. Adams *et. al.*, *Nucl. Phys.* **A757** (2005) 102 [arXiv:nucl-ex/0501009].
2. I. R. Klebanov, arXiv:hep-th/9901018; O. Aharony, S. S. Gubser, J. M. Maldacena, H. Ooguri and Y. Oz, *Phys. Rept.* **323** (2000) 183 [arXiv:hep-th/9905111]; I. R. Klebanov, arXiv:hep-th/0009139; D. T. Son and A. O. Starinets, *Ann. Rev. Nucl. Part. Sci.* **57** (2007) 95 [arXiv:0704.0240 [hep-th]].
3. Y. V. Kovchegov, *Nucl. Phys.* **A830** (2009) 395c [arXiv:0907.4938 [hep-ph]]; E. Iancu, *Acta Phys. Polon.* **B39** (2008) 3213 [arXiv:0812.0500 [hep-ph]]; E. Iancu, *Prog. Theor. Phys. Suppl.* **174** (2008) 306 [arXiv:0807.0489 [hep-ph]]; E. Iancu, *J. Phys.* **G35** (2008) 104059 [arXiv:0805.4110 [hep-th]].

4. K. J. Eskola, K. Kajantie, P. V. Ruuskanen and K. Tuominen, *Nucl. Phys.* **B570** (2000) 379 [arXiv:hep-ph/9909456]; K. J. Eskola, K. Kajantie and K. Tuominen, *Phys. Lett.* **B497** (2001) 39 [arXiv:hep-ph/0009246]; K. J. Eskola, K. Kajantie, P. V. Ruuskanen and K. Tuominen, *Phys. Lett.* **B543** (2002) 208 [arXiv:hep-ph/0204034]; K. J. Eskola, P. V. Ruuskanen, S. S. Rasanen and K. Tuominen, *Nucl. Phys.* **A696** (2001) 715 [arXiv:hep-ph/0104010].
5. N. Armesto, M. A. Braun, E. G. Ferreira and C. Pajares, *Phys. Rev. Lett.* **77** (1996) 3736 [arXiv:hep-ph/9607239]; M. Nardi and H. Satz, *Phys. Lett.* **B442** (1998) 14 [arXiv:hep-ph/9805247]; H. Satz, arXiv:hep-ph/0212046; S. Digal, S. Fortunato, P. Petreczky and H. Satz, *Phys. Lett.* **B549** (2002) 101 [arXiv:hep-ph/0207264]; S. Digal, S. Fortunato and H. Satz, *Eur. Phys. J.* **C32** (2004) 547 [arXiv:hep-ph/0310354]; M. A. Braun, C. Pajares and J. Ranft, *Int. J. Mod. Phys.* **A14** (1999) 2689 [arXiv:hep-ph/9707363].
6. L. V. Gribov, E. M. Levin and M. G. Ryskin, *Phys. Rept.* **100** (1983) 1; A. H. Mueller and J.-w. Qiu, *Nucl. Phys.* **B268** (1986) 427; J. P. Blaizot and A. H. Mueller, *Nucl. Phys.* **B289** (1987) 847.
7. J. Jalilian-Marian, A. Kovner, L. D. McLerran and H. Weigert, *Phys. Rev.* **D55** (1997) 5414 [arXiv:hep-ph/9606337].
8. J. Jalilian-Marian, A. Kovner, A. Leonidov and H. Weigert, *Nucl. Phys.* **B504** (1997) 415 [arXiv:hep-ph/9701284]; J. Jalilian-Marian, A. Kovner, A. Leonidov and H. Weigert, *Phys. Rev.* **D59** (1999) 014014 [arXiv:hep-ph/9706377]; J. Jalilian-Marian, A. Kovner and H. Weigert, *Phys. Rev.* **D59** (1999) 014015 [arXiv:hep-ph/9709432]; J. Jalilian-Marian, A. Kovner, A. Leonidov and H. Weigert, *Phys. Rev.* **D59** (1999) 034007 [arXiv:hep-ph/9807462]; H. Weigert, *Nucl. Phys.* **A703** (2002) 823 [arXiv:hep-ph/0004044]; E. Iancu, A. Leonidov and L. D. McLerran, *Nucl. Phys.* **A692** (2001) 583 [arXiv:hep-ph/0011241]; E. Iancu and L. D. McLerran, *Phys. Lett.* **B510** (2001) 145 [arXiv:hep-ph/0103032]; E. Ferreira, E. Iancu, A. Leonidov and L. McLerran, *Nucl. Phys.* **A703** (2002) 489 [arXiv:hep-ph/0109115]; E. Iancu, A. Leonidov and L. D. McLerran, *Phys. Lett.* **B510** (2001) 133 [arXiv:hep-ph/0102009]; A. H. Mueller, *Phys. Lett.* **B523** (2001) 243 [arXiv:hep-ph/0110169].
9. E. Iancu, A. Leonidov and L. McLerran in *Cargese 2001, QCD perspectives on hot and dense matter*, pp. 74–145. 2002. arXiv:hep-ph/0202270; E. Iancu and R. Venugopalan in *Quark gluon plasma* (R. Hwa and X. N. Wang, eds.). World Scientific, 2003. arXiv:hep-ph/0303204; H. Weigert, *Prog. Part. Nucl. Phys.* **55** (2005) 461 [arXiv:hep-ph/0501087].
10. M. Gyulassy and L. McLerran, *Nucl. Phys.* **A750** (2005) 30 [arXiv:nucl-th/0405013].
11. T. Lappi and L. McLerran, *Nucl. Phys.* **A772** (2006) 200 [arXiv:hep-ph/0602189].
12. A. Kovner, L. D. McLerran and H. Weigert, *Phys. Rev.* **D52** (1995) 3809 [arXiv:hep-ph/9505320].
13. L. D. McLerran and R. Venugopalan, *Phys. Rev.* **D49** (1994) 2233 [arXiv:hep-ph/9309289].
14. S. Jeon and R. Venugopalan, *Phys. Rev.* **D70** (2004) 105012 [arXiv:hep-ph/0406169].
15. A. H. Mueller, *Nucl. Phys.* **A724** (2003) 223 [arXiv:hep-ph/0301109].
16. H. Kowalski, T. Lappi and R. Venugopalan, *Phys. Rev. Lett.* **100** (2008) 022303 [arXiv:0705.3047 [hep-ph]].

17. K. Fukushima, *Phys. Rev.* **D77** (2008) 074005 [arXiv:0711.2364 [hep-ph]].
18. T. Lappi, *Eur. Phys. J.* **C55** (2008) 285 [arXiv:0711.3039 [hep-ph]].
19. J.-P. Blaizot and Y. Mehtar-Tani, *Nucl. Phys.* **A818** (2009) 97 [arXiv:0806.1422 [hep-ph]].
20. T. Altinoluk, A. Kovner, M. Lublinsky and J. Peressutti, *JHEP* **03** (2009) 109 [arXiv:0901.2559 [hep-ph]].
21. T. Altinoluk, A. Kovner and M. Lublinsky, *JHEP* **03** (2009) 110 [arXiv:0901.2560 [hep-ph]].
22. B. Andersson, G. Gustafson, G. Ingelman and T. Sjostrand, *Phys. Rept.* **97** (1983) 31; H. Ehtamo, J. Lindfors and L. D. McLerran, *Z. Phys.* **C18** (1983) 341; T. S. Biro, H. B. Nielsen and J. Knoll, *Nucl. Phys.* **B245** (1984) 449; G. Gatoff, A. K. Kerman and T. Matsui, *Phys. Rev.* **D36** (1987) 114.
23. A. Krasnitz, Y. Nara and R. Venugopalan, *Phys. Rev. Lett.* **87** (2001) 192302 [arXiv:hep-ph/0108092].
24. T. Lappi, *Phys. Rev.* **C67** (2003) 054903 [arXiv:hep-ph/0303076].
25. A. Krasnitz, Y. Nara and R. Venugopalan, *Nucl. Phys.* **A727** (2003) 427 [arXiv:hep-ph/0305112].
26. F. Gelis, T. Lappi and R. Venugopalan, *Phys. Rev.* **D78** (2008) 054019 [arXiv:0804.2630 [hep-ph]].
27. F. Gelis, T. Lappi and R. Venugopalan, *Phys. Rev.* **D78** (2008) 054020 [arXiv:0807.1306 [hep-ph]].
28. D. Kharzeev and M. Nardi, *Phys. Lett.* **B507** (2001) 121 [arXiv:nucl-th/0012025].
29. D. Kharzeev and E. Levin, *Phys. Lett.* **B523** (2001) 79 [arXiv:nucl-th/0108006].
30. I. Balitsky, *Nucl. Phys.* **B463** (1996) 99 [arXiv:hep-ph/9509348].
31. Y. V. Kovchegov, *Phys. Rev.* **D61** (2000) 074018 [arXiv:hep-ph/9905214]; Y. V. Kovchegov, *Phys. Rev.* **D60** (1999) 034008 [arXiv:hep-ph/9901281].
32. F. Gelis, T. Lappi and R. Venugopalan, *Int. J. Mod. Phys.* **E16** (2007) 2595 [arXiv:0708.0047 [hep-ph]].
33. A. Deshpande, R. Milner, R. Venugopalan and W. Vogelsang, *Ann. Rev. Nucl. Part. Sci.* **55** (2005) 165 [arXiv:hep-ph/0506148].
34. J. B. Dainton, M. Klein, P. Newman, E. Perez and F. Willeke, *JINST* **1** (2006) P10001 [arXiv:hep-ex/0603016].
35. N. Armesto, *J. Phys.* **G32** (2006) R367 [arXiv:hep-ph/0604108].
36. H. Kowalski and D. Teaney, *Phys. Rev.* **D68** (2003) 114005 [arXiv:hep-ph/0304189].
37. A. H. Mueller, *Nucl. Phys.* **B415** (1994) 373; A. H. Mueller, *Nucl. Phys.* **B437** (1995) 107 [arXiv:hep-ph/9408245]; A. H. Mueller and B. Patel, *Nucl. Phys.* **B425** (1994) 471 [arXiv:hep-ph/9403256]; B. Andersson, G. Gustafson, A. Nilsson and C. Sjoegren, *Z. Phys.* **C49** (1991) 79; N. N. Nikolaev and B. G. Zakharov, *Z. Phys.* **C49** (1991) 607.
38. M. McDermott, L. Frankfurt, V. Guzey and M. Strikman, *Eur. Phys. J.* **C16** (2000) 641 [arXiv:hep-ph/9912547].
39. S. J. Brodsky, P. Hoyer, N. Marchal, S. Peigne and F. Sannino, *Phys. Rev.* **D65** (2002) 114025 [arXiv:hep-ph/0104291].
40. S. J. Brodsky, R. Enberg, P. Hoyer and G. Ingelman, *Phys. Rev.* **D71** (2005) 074020 [arXiv:hep-ph/0409119].
41. K. J. Golec-Biernat and M. Wusthoff, *Phys. Rev.* **D59** (1999) 014017 [arXiv:hep-ph/9807513].
42. W. Buchmuller, M. F. McDermott and A. Hebecker, *Nucl. Phys.* **B487** (1997) 283

- [arXiv:hep-ph/9607290]; W. Buchmuller, T. Gehrmann and A. Hebecker, *Nucl. Phys.* **B537** (1999) 477 [arXiv:hep-ph/9808454].
43. A. H. Mueller in *Cargese 2001, QCD perspectives on hot and dense matter*, pp. 45–72. 2001. arXiv:hep-ph/0111244.
 44. H. Kowalski, L. Motyka and G. Watt, *Phys. Rev.* **D74** (2006) 074016 [arXiv:hep-ph/0606272].
 45. K. J. Golec-Biernat and M. Wusthoff, *Phys. Rev.* **D60** (1999) 114023 [arXiv:hep-ph/9903358].
 46. A. Dumitru, A. Hayashigaki and J. Jalilian-Marian, *Nucl. Phys.* **A770** (2006) 57 [arXiv:hep-ph/0512129].
 47. F. Gelis and A. Peshier, *Nucl. Phys.* **A697** (2002) 879 [arXiv:hep-ph/0107142].
 48. A. Dumitru and L. D. McLerran, *Nucl. Phys.* **A700** (2002) 492 [arXiv:hep-ph/0105268].
 49. A. Dumitru and J. Jalilian-Marian, *Phys. Lett.* **B547** (2002) 15 [arXiv:hep-ph/0111357].
 50. A. Dumitru and J. Jalilian-Marian, *Phys. Rev. Lett.* **89** (2002) 022301 [arXiv:hep-ph/0204028].
 51. F. Gelis, A. M. Stasto and R. Venugopalan, *Eur. Phys. J.* **C48** (2006) 489 [arXiv:hep-ph/0605087].
 52. **BRAHMS** collaboration, I. Arsene *et. al.*, *Phys. Rev. Lett.* **93** (2004) 242303 [arXiv:nucl-ex/0403005].
 53. J. Jalilian-Marian and Y. V. Kovchegov, *Prog. Part. Nucl. Phys.* **56** (2006) 104 [arXiv:hep-ph/0505052].
 54. A. Dumitru, A. Hayashigaki and J. Jalilian-Marian, *Nucl. Phys.* **A765** (2006) 464 [arXiv:hep-ph/0506308].
 55. D. Kharzeev, E. Levin and L. McLerran, *Phys. Lett.* **B561** (2003) 93 [arXiv:hep-ph/0210332]; J. L. Albacete, N. Armesto, A. Kovner, C. A. Salgado and U. A. Wiedemann, *Phys. Rev. Lett.* **92** (2004) 082001 [arXiv:hep-ph/0307179].
 56. D. Kharzeev, Y. V. Kovchegov and K. Tuchin, *Phys. Rev.* **D68** (2003) 094013 [arXiv:hep-ph/0307037].
 57. J. P. Blaizot, F. Gelis and R. Venugopalan, *Nucl. Phys.* **A743** (2004) 13 [arXiv:hep-ph/0402256]; J. P. Blaizot, F. Gelis and R. Venugopalan, *Nucl. Phys.* **A743** (2004) 57 [arXiv:hep-ph/0402257].
 58. **STAR** collaboration, J. Adams *et. al.*, *Phys. Rev. Lett.* **97** (2006) 152302 [arXiv:nucl-ex/0602011]; **PHENIX** collaboration, S. S. Adler *et. al.*, *Phys. Rev. Lett.* **96** (2006) 222301 [arXiv:nucl-ex/0603017]; **PHENIX** collaboration, Z. Citron, *Nucl. Phys.* **A830** (2009) 607c [arXiv:0907.4796 [nucl-ex]].
 59. **STAR** collaboration, E. Braidot, *Nucl. Phys.* **A830** (2009) 603c [arXiv:0907.3473 [nucl-ex]].
 60. D. Kharzeev, E. Levin and L. McLerran, *Nucl. Phys.* **A748** (2005) 627 [arXiv:hep-ph/0403271]; C. Marquet, *Nucl. Phys.* **B705** (2005) 319 [arXiv:hep-ph/0409023]; R. Baier, A. Kovner, M. Nardi and U. A. Wiedemann, *Phys. Rev.* **D72** (2005) 094013 [arXiv:hep-ph/0506126]; J. Jalilian-Marian, *Eur. Phys. J.* **C61** (2009) 789 [arXiv:0808.2769 [nucl-th]]; K. Tuchin, arXiv:0912.5479 [hep-ph].
 61. C. Marquet, *Nucl. Phys.* **A796** (2007) 41 [arXiv:0708.0231 [hep-ph]].
 62. B. G. Giraud and R. B. Peschanski, *Acta Phys. Polon.* **B37** (2006) 331 [arXiv:math-ph/0504015].
 63. J. Bartels, K. J. Golec-Biernat and H. Kowalski, *Phys. Rev.* **D66** (2002) 014001

- [arXiv:hep-ph/0203258].
64. E. Iancu, K. Itakura and S. Munier, *Phys. Lett.* **B590** (2004) 199 [arXiv:hep-ph/0310338].
 65. H. Kowalski, T. Lappi, C. Marquet and R. Venugopalan, *Phys. Rev.* **C78** (2008) 045201 [arXiv:0805.4071 [hep-ph]].
 66. D. Kharzeev, Y. V. Kovchegov and K. Tuchin, *Phys. Lett.* **B599** (2004) 23 [arXiv:hep-ph/0405045].
 67. K. J. Golec-Biernat, L. Motyka and A. M. Stasto, *Phys. Rev.* **D65** (2002) 074037 [arXiv:hep-ph/0110325]; M. Lublinsky, E. Gotsman, E. Levin and U. Maor, *Nucl. Phys.* **A696** (2001) 851 [arXiv:hep-ph/0102321]; K. J. Golec-Biernat and A. M. Stasto, *Nucl. Phys.* **B668** (2003) 345 [arXiv:hep-ph/0306279]; J. L. Albacete, N. Armesto, J. G. Milhano, C. A. Salgado and U. A. Wiedemann, *Phys. Rev.* **D71** (2005) 014003 [arXiv:hep-ph/0408216]; C. Marquet and G. Soyez, *Nucl. Phys.* **A760** (2005) 208 [arXiv:hep-ph/0504080].
 68. J. L. Albacete, N. Armesto, J. G. Milhano and C. A. Salgado, *Phys. Rev.* **D80** (2009) 034031 [arXiv:0902.1112 [hep-ph]].
 69. J. L. Albacete and C. Marquet, arXiv:1001.1378 [hep-ph].
 70. S. Mrowczynski, *Phys. Rev.* **C49** (1994) 2191; S. Mrowczynski, *Phys. Lett.* **B393** (1997) 26 [arXiv:hep-ph/9606442]; S. Mrowczynski, A. Rebhan and M. Strickland, *Phys. Rev.* **D70** (2004) 025004 [arXiv:hep-ph/0403256]; P. Arnold, J. Lenaghan and G. D. Moore, *JHEP* **08** (2003) 002 [arXiv:hep-ph/0307325]; P. Romatschke and M. Strickland, *Phys. Rev.* **D68** (2003) 036004 [arXiv:hep-ph/0304092]; P. Romatschke and M. Strickland, *Phys. Rev.* **D70** (2004) 116006 [arXiv:hep-ph/0406188]; Y. Nara, *Nucl. Phys.* **A774** (2006) 783 [arXiv:nucl-th/0509052]; A. Dumitru and Y. Nara, *Phys. Lett.* **B621** (2005) 89 [arXiv:hep-ph/0503121]; K. Fukushima, F. Gelis and L. McLerran, *Nucl. Phys.* **A786** (2007) 107 [arXiv:hep-ph/0610416]; K. Fukushima, *Phys. Rev.* **C76** (2007) 021902 [arXiv:0704.3625 [hep-ph]]; P. Romatschke and R. Venugopalan, *Phys. Rev. Lett.* **96** (2006) 062302 [arXiv:hep-ph/0510121]; P. Romatschke and R. Venugopalan, *Phys. Rev.* **D74** (2006) 045011 [arXiv:hep-ph/0605045].
 71. A. Krasnitz and R. Venugopalan, *Nucl. Phys.* **B557** (1999) 237 [arXiv:hep-ph/9809433]; A. Krasnitz and R. Venugopalan, *Phys. Rev. Lett.* **84** (2000) 4309 [arXiv:hep-ph/9909203]; A. Krasnitz and R. Venugopalan, *Phys. Rev. Lett.* **86** (2001) 1717 [arXiv:hep-ph/0007108].
 72. A. Krasnitz, Y. Nara and R. Venugopalan, *Nucl. Phys.* **A717** (2003) 268 [arXiv:hep-ph/0209269].
 73. T. Lappi, *Phys. Rev.* **C70** (2004) 054905 [arXiv:hep-ph/0409328].
 74. T. Lappi, S. Srednyak and R. Venugopalan, *JHEP* **01** (2010) 066 [arXiv:0911.2068 [hep-ph]].
 75. A. H. Mueller, *Nucl. Phys.* **B572** (2000) 227 [arXiv:hep-ph/9906322].
 76. Y. V. Kovchegov, *Nucl. Phys.* **A692** (2001) 557 [arXiv:hep-ph/0011252].
 77. A. H. Mueller, *Nucl. Phys.* **A715** (2003) 20 [arXiv:hep-ph/0208278].
 78. R. Baier, A. H. Mueller, D. Schiff and D. T. Son, *Phys. Lett.* **B539** (2002) 46 [arXiv:hep-ph/0204211].
 79. T. Lappi, *J. Phys.* **G35** (2008) 104052 [arXiv:0804.2338 [hep-ph]].
 80. A. Freund, K. Rummukainen, H. Weigert and A. Schafer, *Phys. Rev. Lett.* **90** (2003) 222002 [arXiv:hep-ph/0210139].
 81. N. Armesto, C. A. Salgado and U. A. Wiedemann,

44 *T. Lappi*

- Phys. Rev. Lett.* **94** (2005) 022002 [arXiv:hep-ph/0407018].
82. J. L. Albacete, *Phys. Rev. Lett.* **99** (2007) 262301 [arXiv:0707.2545 [hep-ph]].
83. M. L. Miller, K. Reygers, S. J. Sanders and P. Steinberg, *Ann. Rev. Nucl. Part. Sci.* **57** (2007) 205 [arXiv:nucl-ex/0701025].
84. T. Lappi and R. Venugopalan, *Phys. Rev.* **C74** (2006) 054905 [arXiv:nucl-th/0609021].
85. H. J. Drescher and Y. Nara, *Phys. Rev.* **C75** (2007) 034905 [arXiv:nucl-th/0611017].
86. H.-J. Drescher and Y. Nara, *Phys. Rev.* **C76** (2007) 041903 [arXiv:0707.0249 [nucl-th]].
87. P. Sorensen, arXiv:0905.0174 [nucl-ex].
88. P. F. Kolb, U. W. Heinz, P. Huovinen, K. J. Eskola and K. Tuominen, *Nucl. Phys.* **A696** (2001) 197 [arXiv:hep-ph/0103234].
89. T. Hirano, U. W. Heinz, D. Kharzeev, R. Lacey and Y. Nara, *Phys. Lett.* **B636** (2006) 299 [arXiv:nucl-th/0511046].
90. H.-J. Drescher, A. Dumitru, A. Hayashigaki and Y. Nara, *Phys. Rev.* **C74** (2006) 044905 [arXiv:nucl-th/0605012].
91. A. Kuhlman, U. W. Heinz and Y. V. Kovchegov, *Phys. Lett.* **B638** (2006) 171 [arXiv:nucl-th/0604038].
92. H.-J. Drescher, A. Dumitru, C. Gombeaud and J.-Y. Ollitrault, *Phys. Rev.* **C76** (2007) 024905 [arXiv:0704.3553 [nucl-th]].
93. **STAR** collaboration, P. Sorensen, *J. Phys.* **G35** (2008) 104102 [arXiv:0808.0356 [nucl-ex]]; **PHOBOS** collaboration, B. Alver *et. al.*, *J. Phys.* **G35** (2008) 104101 [arXiv:0804.4297 [nucl-ex]].
94. **STAR** collaboration, B. I. Abelev *et. al.*, *Phys. Rev. Lett* **103** (2009) 172301 [arXiv:0905.0237 [nucl-ex]].
95. **STAR** collaboration, B. I. Abelev *et. al.*, *Phys. Rev.* **C80** (2009) 064912 [arXiv:0909.0191 [nucl-ex]].
96. **STAR** collaboration, J. Adams *et. al.*, *Phys. Rev.* **C73** (2006) 064907 [arXiv:nucl-ex/0411003]; **STAR** collaboration, M. Daugherty, *J. Phys.* **G35** (2008) 104090 [arXiv:0806.2121 [nucl-ex]].
97. J. Putschke, *J. Phys.* **G34** (2007) S679 [arXiv:nucl-ex/0701074]; **PHOBOS** collaboration, B. Alver *et. al.*, *J. Phys.* **G35** (2008) 104080 [arXiv:0804.3038 [nucl-ex]]; **PHOBOS** collaboration, B. Alver *et. al.*, arXiv:0812.1172 [nucl-ex]; J. L. Nagle, *Nucl. Phys.* **A830** (2009) 147c [arXiv:0907.2707 [nucl-ex]].
98. T. J. Tarnowsky, arXiv:0807.1941 [nucl-ex].
99. T. Lappi and L. McLerran, *Nucl. Phys.* **A832** (2010) 330 [arXiv:0909.0428 [hep-ph]].
100. **STAR** collaboration, S. A. Voloshin, arXiv:0806.0029 [nucl-ex]; **STAR** collaboration, S. A. Voloshin, *Nucl. Phys.* **A830** (2009) 377c [arXiv:0907.2213 [nucl-ex]].
101. **STAR** collaboration, B. I. Abelev *et. al.*, *Phys. Rev. Lett.* **103** (2009) 251601 [arXiv:0909.1739 [nucl-ex]]; **STAR** collaboration, B. I. Abelev, arXiv:0909.1717 [nucl-ex].
102. F. Gelis and R. Venugopalan, *Nucl. Phys.* **A776** (2006) 135 [arXiv:hep-ph/0601209]; F. Gelis and R. Venugopalan, *Nucl. Phys.* **A779** (2006) 177 [arXiv:hep-ph/0605246].
103. K. Fukushima and Y. Hidaka, *Nucl. Phys.* **A813** (2008) 171

- [arXiv:0806.2143 [hep-ph]].
104. N. Armesto, L. McLerran and C. Pajares, *Nucl. Phys.* **A781** (2007) 201 [arXiv:hep-ph/0607345].
 105. A. Dumitru, F. Gelis, L. McLerran and R. Venugopalan, *Nucl. Phys.* **A810** (2008) 91 [arXiv:0804.3858 [hep-ph]].
 106. K. Dusling, D. Fernandez-Fraile and R. Venugopalan, *Nucl. Phys.* **A828** (2009) 161 [arXiv:0902.4435 [nucl-th]].
 107. F. Gelis, T. Lappi and L. McLerran, *Nucl. Phys.* **A828** (2009) 149 [arXiv:0905.3234 [hep-ph]].
 108. **UA1** collaboration, G. Arnison *et. al.*, *Phys. Lett.* **B123** (1983) 108; **UA5** collaboration, G. J. Alner *et. al.*, *Phys. Lett.* **B160** (1985) 193; **UA5** collaboration, G. J. Alner *et. al.*, *Phys. Lett.* **B160** (1985) 199; **UA5** collaboration, R. E. Ansorge *et. al.*, *Z. Phys.* **C37** (1988) 191; **PHENIX** collaboration, S. S. Adler *et. al.*, *Phys. Rev.* **C76** (2007) 034903 [arXiv:0704.2894 [nucl-ex]]; **PHENIX** collaboration, A. Adare *et. al.*, *Phys. Rev.* **C78** (2008) 044902 [arXiv:0805.1521 [nucl-ex]].
 109. K. Fukushima, F. Gelis and T. Lappi, *Nucl. Phys.* **A831** (2009) 184 [arXiv:0907.4793 [hep-ph]].
 110. S. Gavin, L. McLerran and G. Moschelli, *Phys. Rev.* **C79** (2009) 051902 [arXiv:0806.4718 [nucl-th]].
 111. S. A. Voloshin, *Phys. Lett.* **B632** (2006) 490 [arXiv:nucl-th/0312065]; E. V. Shuryak, *Phys. Rev.* **C76** (2007) 047901 [arXiv:0706.3531 [nucl-th]]; C. A. Pruneau, S. Gavin and S. A. Voloshin, *Nucl. Phys.* **A802** (2008) 107 [arXiv:0711.1991 [nucl-ex]].
 112. G. Moschelli and S. Gavin, arXiv:0910.3590 [nucl-th].
 113. D. Kharzeev, R. D. Pisarski and M. H. G. Tytgat, *Phys. Rev. Lett.* **81** (1998) 512 [arXiv:hep-ph/9804221]; D. Kharzeev and R. D. Pisarski, *Phys. Rev.* **D61** (2000) 111901 [arXiv:hep-ph/9906401]; D. Kharzeev, *Phys. Lett.* **B633** (2006) 260 [arXiv:hep-ph/0406125].
 114. D. Kharzeev, A. Krasnitz and R. Venugopalan, *Phys. Lett.* **B545** (2002) 298 [arXiv:hep-ph/0109253].
 115. D. E. Kharzeev, L. D. McLerran and H. J. Warringa, *Nucl. Phys.* **A803** (2008) 227 [arXiv:0711.0950 [hep-ph]]; K. Fukushima, D. E. Kharzeev and H. J. Warringa, *Phys. Rev.* **D78** (2008) 074033 [arXiv:0808.3382 [hep-ph]]; D. E. Kharzeev and H. J. Warringa, *Phys. Rev.* **D80** (2009) 034028 [arXiv:0907.5007 [hep-ph]]; K. Fukushima, D. E. Kharzeev and H. J. Warringa, arXiv:0912.2961 [hep-ph].
 116. F. Wang, arXiv:0911.1482 [nucl-ex]; A. Bzdak, V. Koch and J. Liao, arXiv:0912.5050 [nucl-th]; S. Pratt, arXiv:1002.1758 [nucl-th].
 117. K. Dusling, F. Gelis, T. Lappi and R. Venugopalan, arXiv:0911.2720 [hep-ph].
 118. F. Gelis, T. Lappi and R. Venugopalan, *Phys. Rev.* **D79** (2008) 094017 [arXiv:0810.4829 [hep-ph]].
 119. T. Lappi, *Acta Phys. Polon.* **B40** (2009) 1997 [arXiv:0904.1670 [hep-ph]].
 120. J.-P. Blaizot, E. Iancu and H. Weigert, *Nucl. Phys.* **A713** (2003) 441 [arXiv:hep-ph/0206279].
 121. K. Rummukainen and H. Weigert, *Nucl. Phys.* **A739** (2004) 183 [arXiv:hep-ph/0309306].
 122. Y. V. Kovchegov, J. Kuokkanen, K. Rummukainen and H. Weigert, *Nucl. Phys.* **A823** (2009) 47 [arXiv:0812.3238 [hep-ph]].